



Deposited via The University of Sheffield.

White Rose Research Online URL for this paper:

<https://eprints.whiterose.ac.uk/id/eprint/182984/>

Version: Accepted Version

---

**Article:**

Ren, J., Zhang, L., Walkley, B. et al. (2022) Degradation resistance of different cementitious materials to phosphoric acid attack at early stage. *Cement and Concrete Research*, 151. 106606. ISSN: 0008-8846

<https://doi.org/10.1016/j.cemconres.2021.106606>

---

© 2021 Published by Elsevier Ltd. This is an author produced version of a paper subsequently published in *Cement and Concrete Research*. Uploaded in accordance with the publisher's self-archiving policy. Article available under the terms of the CC-BY-NC-ND licence (<https://creativecommons.org/licenses/by-nc-nd/4.0/>).

**Reuse**

This article is distributed under the terms of the Creative Commons Attribution-NonCommercial-NoDerivs (CC BY-NC-ND) licence. This licence only allows you to download this work and share it with others as long as you credit the authors, but you can't change the article in any way or use it commercially. More information and the full terms of the licence here: <https://creativecommons.org/licenses/>

**Takedown**

If you consider content in White Rose Research Online to be in breach of UK law, please notify us by emailing [eprints@whiterose.ac.uk](mailto:eprints@whiterose.ac.uk) including the URL of the record and the reason for the withdrawal request.

# Degradation resistance of different cementitious materials to phosphoric acid attack at early stage

Jie Ren<sup>1,2</sup>, Lihai Zhang<sup>1</sup>, Brant Walkley<sup>3</sup>, Jay R. Black<sup>4</sup>, Rackel San Nicolas<sup>1\*</sup>

<sup>1</sup> Department of Infrastructure Engineering, the University of Melbourne, Victoria, 3010, Australia

<sup>2</sup> Guangdong Provincial Key Laboratory of Durability for Marine Civil Engineering, College of Civil and Transportation Engineering, Shenzhen University, Shenzhen 518060, China

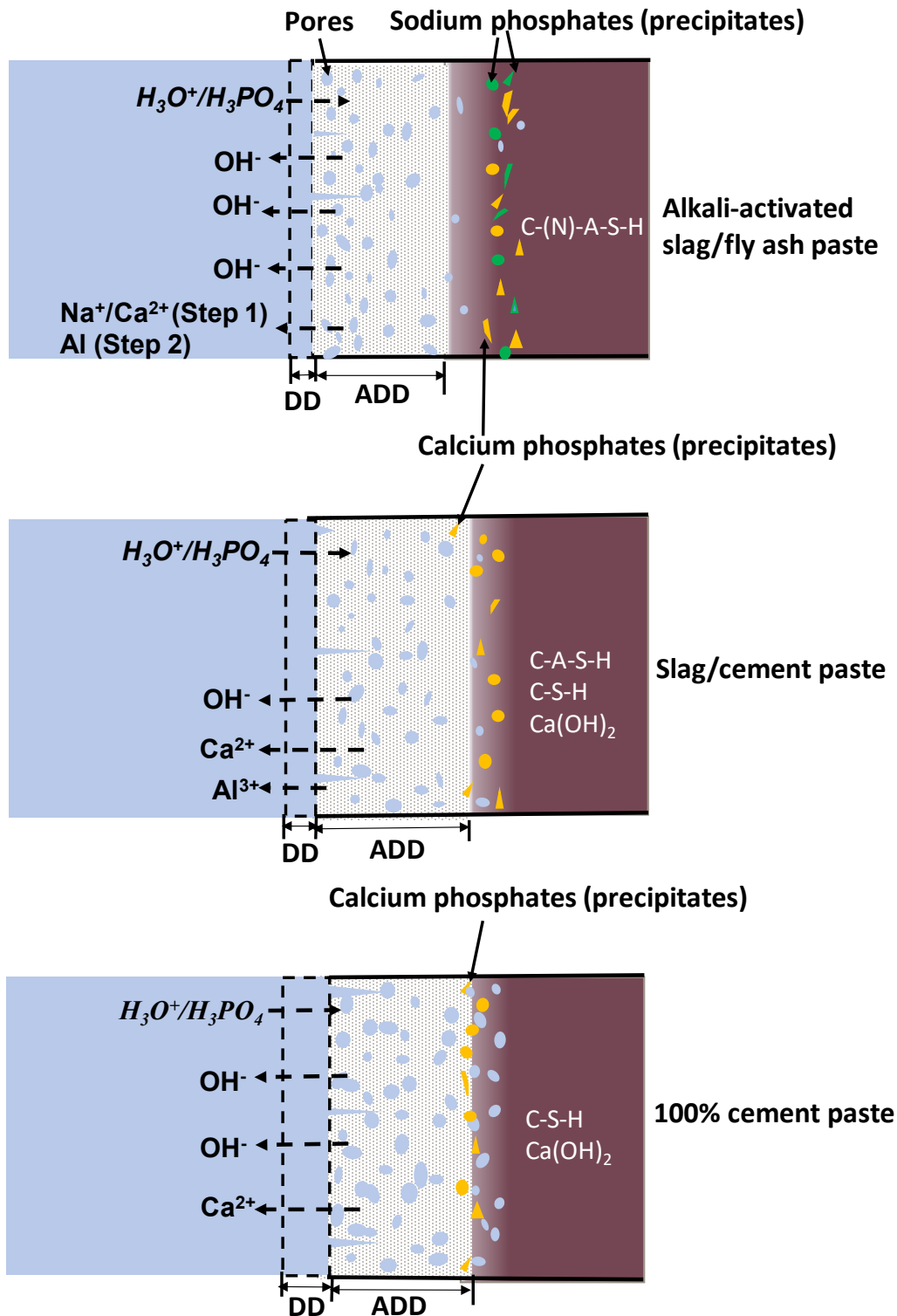
<sup>3</sup> Department of Chemical and Biological Engineering, The University of Sheffield, Sheffield S1 3JD, UK

<sup>4</sup> School of Earth Sciences, Peter Cook Centre for CCS Research, The University of Melbourne, VIC 3010 Australia

## Abstract

Sewer wastewater systems pose great threats to OPC-based concretes used for pipes due to the presence of various acids. Phosphoric acid can cause as much damage as sulphuric acid but has been very lightly studied. This study focuses on the early stage of the degradation process of different cementitious materials in phosphoric acid. Three types of cementitious materials are compared: OPC (100% cement), slag-blended OPC (slag/cement mass ratio at 65/35) and alkali-activated slag/fly ash pastes (slag/fly ash mass ratio at 50/50). Samples were exposed to phosphoric acid solution with a constant pH at  $2.0 \pm 0.2$  for 44 days. The degradation kinetics, chemical and microstructural properties as well as dissolution rate of these binders are analysed. The results show that the alkali-activated slag/fly ash binder has the lowest degradation rate compared to the other cement-based binders. The intrinsic characteristics of the binders lead to significant changes in the kinetics of degradation. The chemical properties of the binders are the critical influential factor of the early stage behaviour. A conceptual degradation process is proposed to describe the early-stage kinetics of degradation for the cementitious materials studied.

**Keywords:** Phosphoric acid; Early stage; Alkali-activated slag/fly ash binders; Degradation resistance



29 **Graphical abstract**

30 Schematic diagram showing the early stage degradation processes of AASF and OPC-based  
 31 pastes exposed to the phosphoric acid. ADD-Apparent degradation depth; DD-  
 32 Dissolved/detached depth.

## 33 1. Introduction

34 The resistance of cementitious materials exposed to acidic environments, such as sewage  
35 wastewater pipes containing effluents, has seen a recent growth in academic and industrial  
36 interest [1-14] due to immense costs of maintaining this infrastructure. When exposed to acidic  
37 agro-industrial wastewaters, cementitious materials suffer from severe deterioration due to  
38 reactions between their alkaline matrix and various acids [15-19].

39 Phosphates ( $\text{H}_2\text{PO}_4^-$ ,  $\text{HPO}_4^{2-}$  or  $\text{PO}_4^{3-}$ ), are one of the main components in silage effluent  
40 discharged by agricultural practices with a resultant acidic condition ( $\text{pH} \approx 3.5-5$ ) [20], posing  
41 severe challenges for cementitious materials used in sewer networks [8, 21, 22]. According to  
42 related research [23], fertilizer production could produce a dilute mixture of phosphoric,  
43 sulfuric and even fluosilic acids with pH level as low as 1 to 2. Previous studies have shown  
44 that the exposure of OPC concretes to phosphoric acid ( $\text{pH} = 2, 3$  or  $4$ ) or phosphate-rich acidic  
45 environments resulted in significant degradation [1, 8, 24].

46 It has been reported that the degradation process of cementitious binders caused by acid  
47 attacks is a synergistic effect of chemical reactions which generally dominate early stage  
48 degradation and physical ion diffusion which is more obvious during later stages [25, 26].  
49 Specially, chemical reactions occur at the surface of cementitious binders first, forming  
50 different chemical products and a degraded layer. With the thickness of the degraded layer  
51 gradually increasing, the acid solution has to diffuse the degraded layer before reaching  
52 undegraded components and triggering new reactions. It is apparent the early stage degradation  
53 process is critical for the entire performance of cementitious binders as it determines the  
54 reaction products, i.e. different types of calcium salts, and formation of degraded layer which  
55 could significantly influence the subsequent degradation evolutions [16, 27, 28]. Despite recent  
56 advances, there remains a lack of understanding of the degradation effect and related  
57 mechanisms of phosphoric acid on cementitious materials, particularly during early stages.

58 Alkali-activated materials (AAMs) are a viable alternative with potential to replace OPC-  
59 based binders due to their lower  $\text{CO}_2$  footprint, comparable mechanical strength and enhanced  
60 durability, especially acid resistance compared to their OPC counterparts. Among all types of  
61 AAMs, alkali-activated slag/fly ash (AASF) has become more appealing due to some  
62 disadvantages and limitations when only fly ash (FA) or slag is used [29-32]. Specifically, the  
63 use of FA as the only precursor often requires heat curing to achieve structural integrity at early  
64 ages [33], which is not practical for in-situ industrial applications. For alkali-activated slag, the  
65 main reaction product after hydration reaction is an aluminium-substituted calcium silicate

66 hydrate gel (C-(A)-S-H gel) with a low Ca/Si ratio [34]. This type of gel is reported to be more  
67 susceptible towards acidic degradation due to its higher calcium content as compared to the  
68 sodium aluminosilicate hydrate (N-A-S-H) type gels in FA-based AAMs [35, 36]. In  
69 comparison, AASF binders contain both C-(A)-S-H and N-A-S-H gels [37-39] which are  
70 expected to mitigate the abovementioned problems that single slag or FA-based AAMs have.

71 Durability of AASF binders in acid environments has been partially investigated in some  
72 literature and it is confirmed that although AASF binders generally have a certain resistance  
73 capacity towards some acid attacks such as sulphuric and nitric, they may still suffer from  
74 deteriorations such as the formation of a degraded product layer along with corroded depth.  
75 “Corroded depth” is here defined as in some literature as an area with lower pH and other  
76 possible change in the nature of the binder [40-42]. However, related research focusing on their  
77 behaviour under phosphoric acid attack and detailed comparisons with OPC-based binders is  
78 far from adequate [8].

79 This study aims to investigate the early stage degradation of AASF (slag/FA = 1 by mass)  
80 in phosphoric acid solutions and another two types of OPC-based binders are used as references.  
81 The blended OPC binder usage is based on studies [19, 43] which reported that supplementary  
82 cementitious materials rich in Al (such as slag in this study) could improve the acid resistance  
83 by improving the microstructure and integrity of degraded layers. Various indicators including  
84 degradation depth, mass changes and leaching rates of ions were employed in the study to  
85 monitor the degradation kinetics. Chemical and microstructural analysis were also used to  
86 characterise their resistance to degradation by phosphoric acid at early stages. Finally,  
87 conceptual descriptions of the degradation for all binders are proposed.

## 88 **2. Materials and methods**

### 89 **2.1. Materials**

90 A type of FA (class F) according to ASTM C618 was used as precursors for AASF binders,  
91 supplied by CEMENT AUSTRALIA. The slag used in this study is ground granulated blast  
92 furnace slag (GGBFS) from Independent Cement and Lime Pty Ltd., also used as a precursor  
93 for AASF binders. In the rest of the manuscript the term slag will be used for GGBFS. The FA  
94 and slag has a specific gravity of 2,800 and 2,200 kg/m<sup>3</sup> respectively and their corresponding  
95 median particle size (d<sub>50</sub>) was 14 for FA and 25 µm for slag. A GP (General purpose) type OPC  
96 (Eureka Cement, Australia) in accordance with AS 3972 with a specific gravity between 2,800-  
97 3,200 kg/m<sup>3</sup> and bulk density 1,200-1,600 kg/m<sup>3</sup> was used. Their chemical compositions and  
98 X-ray diffraction (XRD) patterns are shown in Table 1 and Fig. 1 (FA and slag) and Fig. 2 (OPC),

99 respectively. According to Fig. 1, FA contains some crystalline phases such as mullite, quartz  
 100 and hematite. In comparison, slag was mainly amorphous evidenced by a broad diffuse hump  
 101 between 25 and 35 ° (2θ) with a few Akermanite and gypsum. Generally, OPC is composed of  
 102 alite, belite and gypsum as well as ferrite which are also observed in Fig. 2. Anhydrous sodium  
 103 metasilicate powder (Na<sub>2</sub>SiO<sub>3</sub>) with SiO<sub>2</sub>:Na<sub>2</sub>O molar ratio at 1:1 was selected as the solid  
 104 alkaline activator which was provided by Redox Pty Ltd. Tap water was used as the mixing  
 105 water. Phosphoric acid solution was synthesised by mixing distilled water and analytical  
 106 reagent-grade ortho-phosphoric acid (85% w/w, 1.71 g/mL), provided by Chem-supply.

107 **Table 1**

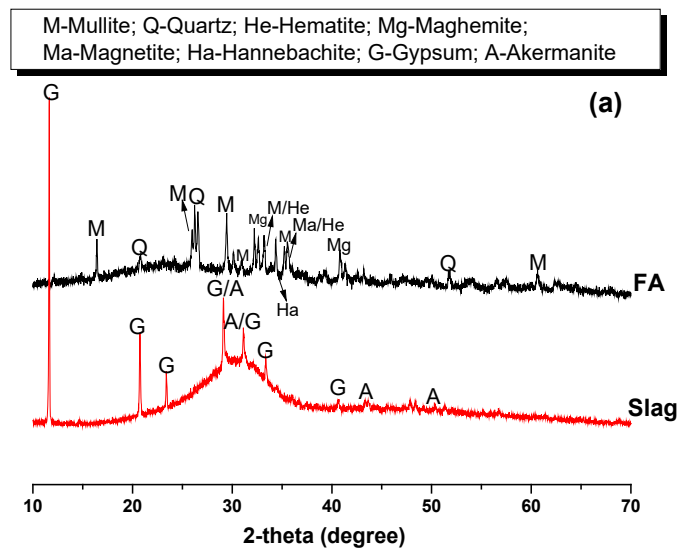
108 Chemical compositions of the FA, Slag and OPC used (wt.%), as determined by X-ray  
 109 fluorescence.

110 \* LOI refers to loss on ignition at 1,000 °C.

Precursor	Component (mass % as oxide)										
	SiO <sub>2</sub>	TiO <sub>2</sub>	Al <sub>2</sub> O <sub>3</sub>	Fe <sub>2</sub> O <sub>3</sub>	MnO	MgO	CaO	K <sub>2</sub> O	P <sub>2</sub> O <sub>5</sub>	SO <sub>3</sub>	LOI*
Slag	31.00	0.49	13.96	0.32	0.33	6.33	40.92	0.31	0.01	2.17	2.11
FA	42.09	1.44	25.13	13.16	0.18	1.27	13.56	0.41	1.10	0.41	0.81
OPC	20.34	-	4.47	4.58	-	1.24	62.91	0.29	-	2.58	3.27

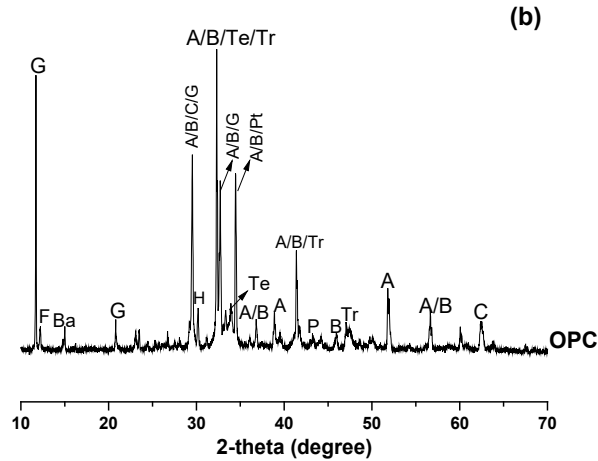
111

112



113

A-Alite( $C_3S$ ); B-Belite( $C_2S$ ); C-Calcite; Te- $C_4AF$ ; Tr- $C_3A$ ; H-Hemihydrate;  
G-Gypsum; P-Periclase; F-Ferrite; Ba-Bassanite; Pt-Portlandite



114

115

Fig. 1. XRD spectra of the raw materials: (a) Slag and FA; (b) OPC.

116

## 2.2. Preparation of AASF and OPC-based pastes

117

118

119

120

121

122

123

124

125

126

127

128

129

130

131

132

133

134

135

136

137

The AASF paste was prepared by mixing the slag and FA dry powders first in a Hobart mixer for two minutes before adding the alkaline activator solution which was made by stirring the  $Na_2SiO_3$  and required water in a beaker, then covered with a watch glass to minimise evaporation and followed by cooling down naturally to room temperature. The mixture was mixed for 8 minutes, cast in two layers into 50 mm cubic moulds or cylinder moulds ( $\Phi$  27.5 mm  $\times$  H 55 mm) and compacted carefully on a vibrating table for two minutes to remove introduced air bubbles during the mixing process. The newly-mixed pastes were cured at  $23 \pm 2$  °C with plastic films covered on casting surfaces to minimise moisture loss. After 24 hours, all specimens were demoulded, sealed tightly in plastic bags and stored immediately in a cabinet at room temperature ( $23 \pm 2$  °C) until further testing. For OPC-based pastes, a pilot study was carried out in order to achieve similar compressive strength compared to that of the AASF paste. Pure 100% OPC paste and blended OPC with slag were manufactured with the predetermined water-to-binder ratio at 0.38 and 0.40 respectively. The mixing procedure was similar compared to AASF pastes but the curing condition was different: OPC-based pastes were all cured in water with the same laboratory condition (temperature =  $23 \pm 2$  °C). Detailed denotations and mix proportions of the three mixes are tabulated in Table 2. Paste samples were used throughout the study and were cured for 56 days to ensure a complete hydration process prior to acid immersions and other tests. It is noteworthy that pastes not mortar or concrete specimens were made for comparison because we mainly deal with the intrinsic stabilities of different binding components in various binders when suffering from acid attacks without considering interfacial transition zone.

138 **Table 2**

139 Mix proportions of the three types of binder mixes in the study.

Sample code	Composition (%) of the binder	Water/binder ratio	Solid activator dosage (%)
50Slag 50FA	slag: FA = 50:50	0.342	8
65Slag 35OPC	slag: OPC = 65:35	0.40	-
100OPC	OPC: 100	0.38	-

140 All ratios and percentages are expressed in mass.

141 **2.3. Test procedure**

142 **2.3.1. Initial properties before acid immersion**

143 Water absorption accompanied with volume of permeable voids (VPV) and capillary  
 144 sorptivity of the paste specimens after 56 days of curing[44] were measured according to  
 145 ASTM C642-06 [45] and ASTM C1585-04 [46], respectively. The preconditioning  
 146 temperature for the water absorption and VPV, and capillary sorptivity test was 60 °C and 50 °C  
 147 respectively because higher temperatures may alter the microstructures of alkali-activated  
 148 binders [44]. Final results were expressed as an average of three specimens for each mix. The  
 149 compressive strength after 56-day curing was tested on the 50 mm cubic samples in triplicates  
 150 using an ELE International tester with a loading rate at 0.9 kN/s in compliance with the ASTM  
 151 C109/C109M-12 (2012) [47].

152

153 **2.3.2. Phosphoric acid immersion**

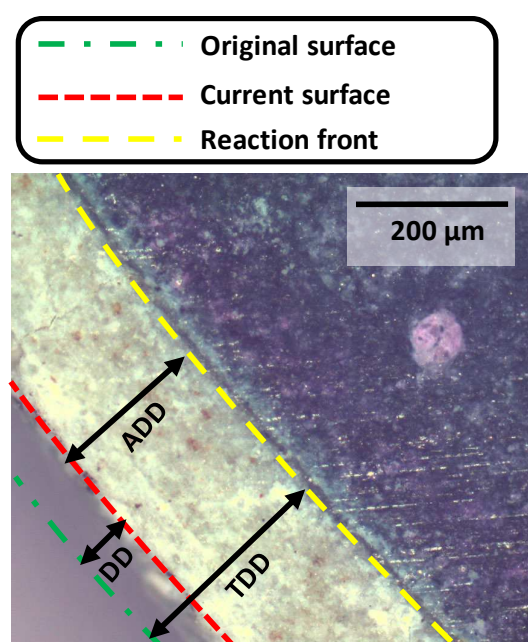
154 In this study, for each binder mix, six cylindrical samples were fully immersed in separated  
 155 containers with 1 L phosphoric acid (pH  $2.0 \pm 0.2$  most of the time) for 44 days. The pH was  
 156 kept as constant as possible by replacing the phosphoric acid solution based on predetermined  
 157 intervals. Specifically, the solution was replaced every day during the first 7 days. Within this  
 158 period the pH tends to increase quickly up to pH=4 in the first 24 hours in worst cases. After 3  
 159 days these increases are reduced 0.5 then 0.2 after 7 days. After 7 days none of the solutions  
 160 were having as much variation and the solution were change only every second day until 14  
 161 days of immersion to keep the pH at  $2 \pm 0.2$ . From 14 days, the solutions were renewed every  
 162 three days until the end of the acid immersion (44 days) to maintain the pH at  $2 \pm 0.2$ . The solid  
 163 surface/liquid volume was approximately  $0.29 \text{ cm}^{-1}$  and solid/liquid volume ratio was 0.20  
 164 throughout the immersion period. The pH level was selected based on the scenarios where  
 165 concrete structures are applied in sewage wastewater pipes, food process or mining industries  
 166 [48-50]. The top and bottom surfaces of the specimens were sealed using inert silica gel to

167 ensure a horizontal direction of acid ingress and the corresponding experimental setup can be  
168 referred to the literature [8]. Another batch of specimens were submerged in distilled water as  
169 a reference which was also regularly replaced with the same renewal frequency as the  
170 phosphoric acid solution. In order to quantify the alkalinity of pore solutions of the three binder  
171 mixes, the continuous pH changes over the first day of immersion before renewal of acid or  
172 water were monitored using HI 3222 pH/ORP/ISE meter with an accuracy of 0.01. This  
173 measurement was only conducted within one day of immersion because the greatest pH  
174 changes occur within one-day of immersion [35, 51]. It is worth pointing out that unless further  
175 introductions, this exposure regime applies to the samples for all measurements

### 176 2.3.3. Degradation kinetic measurements

#### 177 *Degradation depth*

178 Total degradation depth (TDD), simplified as degradation depth was used as the direct  
179 indicator of degradation kinetics which is a numerical combination of dissolved/detached depth  
180 (DD) [16] due to partial dissolution and/or detachment of specimens in acid solution and  
181 apparent degradation depth (ADD) as indicated by phenolphthalein colouration method. A  
182 presentation of the TDD, DD and ADD after the spray of phenolphthalein solution is shown in  
183 Fig. 2. This method, based on DIN EN 14630:2007-01, has been widely used as a reliable  
184 indicator of various degradation processes [36, 52-55]. The detailed description of the  
185 degradation depth measurement is introduced in the following references [8, 24]. The  
186 measurements were conducted on small disks cut from 6 parallel specimens which were  
187 continuously submerged in the acid solution throughout the entire immersion period.



189 **Fig. 2.** An image of a disk-shaped sample cross-section after phenolphthalein spray showing the  
190 determination of total degradation depth (TDD), ADD and DD.

### 191 *Mass changes*

192 Mass changes were examined before each measurement of degradation depth. At each  
193 sampling stage, specimens were taken out from the phosphoric acid solution gently and dried  
194 slightly using a wet cloth before weighing to remove surface water. The whole weighing  
195 process was completed within 30 seconds to minimize the water evaporation from sample  
196 surfaces using a digital scale with a precision of  $\pm 0.01$  g. Samples were then positioned back  
197 into the phosphoric acid solutions. At the same time, mass changes of the references submerged  
198 in distilled water were also recorded.

### 199 *Leaching rates of related ions*

200 Concentrations of different elements including Ca, Na, Al and Si in the phosphoric acid  
201 solution were analysed by Inductively coupled plasma-optical emission spectrometer (ICP-  
202 OES) analyser (Optima 4400, Perkin Elmer, USA). Three cylindrical samples ( $\Phi$  27.5 mm  $\times$   
203 H 55 mm with volume of 32.65 cm<sup>3</sup>) of each mix was immersed in 900 mL phosphoric acid  
204 solution separately with the same pH level ( $2.0 \pm 0.2$ ). The solid/liquid volume ratio was 0.11  
205 for all mixes because a higher ratio could lead to the concentrations of ions above the testing  
206 limits. The renewal of acid occurred right after 3, another 4 (7 days in total), another 3 (10 days  
207 in total), and another 4 (14 days in total) days of immersion, the frequency of which was lower  
208 than that of the degradation depth measurements because of a smaller solid/liquid volume ratio  
209 used in this test. The concentrations of Ca, Na, Al, Si, released out from the specimens in the  
210 corresponding leachate phosphoric acid solutions were measured right before each renewal of  
211 acid, namely after a total of 3, 7, 10 and 14 days as well as 21 days by the end of the immersion.  
212 This test helps to follow the kinetics of ions mobility even the conditions are not exactly the  
213 same than the ones in other tests.

### 214 **2.3.4. Mineralogical, chemical and microstructural analysis**

215 Mineralogical and chemical characteristics of both degraded and undegraded part of  
216 specimens were evaluated using X-ray diffraction analysis (XRD), thermogravimetric analysis  
217 (TGA), derivative thermogravimetry (DTG) and environmental scanning electron microscope  
218 equipped with energy dispersive X-ray spectroscopy (ESEM/EDS). Micro X-ray computed  
219 tomography ( $\mu$ -XCT) was also used to provide non-destructive three-dimensional (3D)  
220 microstructural information on the degraded and undegraded regions of the specimens.

221 Crushed samples from both degraded and undegraded parts of the specimens after 44-day  
222 immersion were grounded into fine powders (passing through the 75  $\mu\text{m}$  sieve (No.200))  
223 followed by drying in a desiccator for 24 hours at room temperature prior to XRD and  
224 TGA/DTG tests. For ESEM/EDS, samples after 14-day immersion were first pre-heated at 60  
225  $^{\circ}\text{C}$  for 48 hours to expel all moisture and then sectioned including both degraded and  
226 undegraded part, impregnated with epoxy resin and polished using SiC abrasive paper prior to  
227 the analysis. The 3D microstructures of a piece of specimens cut off from the sample surface  
228 after 21-day immersion were examined using XCT. The dimension of each binder mix was  
229 around 1 mm in width and length to obtain a high resolution (1.77  $\mu\text{m}$ ). The 14-day and 21-  
230 day testing point was selected because the degradation performance is discernible enough after  
231 these immersion periods, shortly after the induction stage for the 50Slag\_50FA sample.

232 XRD patterns were recorded using a Bruker D8 Advance diffractometer with Cu –  $K\alpha$   
233 radiation and data were collected in a  $2\theta$  range of  $10\text{-}70^{\circ}$ . The scanning rate was  $1.2^{\circ}/\text{min}$ .  
234 TGA/DTG was carried out in a PerkinElmer Diamond instrument. ESEM was conducted using  
235 an FEI Quanta instrument with a 15 kV accelerating voltage and the working distance was 10  
236 mm. EDS was run by a Link-Isis (Oxford Instruments) X-ray energy dispersive detector for  
237 chemical composition analysis. Micro-CT analysis was performed with a Phoenix Nanotom m  
238 (Waygate Technologies) operated using xs control and Phoenix datos|x acquisition  
239 reconstruction software (both Waygate Technologies). Micro-CT scans were collected over  
240 47.5 minutes using an x-ray energy of 60 kV and 240  $\mu\text{A}$  collecting 1400 x-ray projections  
241 through a full 360 degrees of rotation. Reconstructed data was exported in a 16-bit format and  
242 imported to Avizo (Thermo Fisher Scientific) for analysis.

### 243 **2.3.5. Intrinsic acid resistance measurement**

244 In order to eliminate the influence of porous structure on the acid resistance of different  
245 cementitious binders, specimens were ground to fine powders (size  $< 90 \mu\text{m}$ ). Then they were  
246 immersed in a nitric acid solution (approximately 0.06 wt.%,  $\text{pH} = 2.0 \pm 0.2$ ) to avoid possible  
247 clogging effect that may happen to other acids because nitrates are highly soluble without any  
248 precipitation [56]. For each mix, 0.2 g powders were firstly immersed in 200 mL nitric acid  
249 solution and then constantly stirred for one minute followed by natural deposition in ambient  
250 environment. This small amount of powder but large volume of acid solution was employed to  
251 avoid the need for acid renewal due to pH changes. After 48-hour immersion, three suspension  
252 solutions for different mixes were vacuum filtered by gravity filter paper (8  $\mu\text{m}$  in pore size).  
253 The powders on the filter paper were then rinsed with deionised water completely until a neutral

254 pH was obtained. After that, the insoluble residue powders were dried at 50 °C for at least 3  
255 days to remove any moisture until a constant mass was achieved. Finally, the residue powder  
256 was weighed to calculate the dissolution rate (DR) using the following equation:

$$257 \quad DR = \frac{M_{\text{before}} - M_{\text{after}}}{M_{\text{before}}} \quad (1)$$

258 where  $M_{\text{before}}$  and  $M_{\text{after}}$  refers to the mass before immersion and the dry mass of residual  
259 powders respectively. In this study,  $M_{\text{before}}$  is approximately 0.2 g for all binder mixes. The  
260 measurement was repeated twice.

261 Since the dissolution rate is highly dependent on the surface area of reactants [57], the  
262 surface area of the initial powdered sample after 56 days of curing was also quantified by  
263 performing Brunauer-Emmett-Teller (BET) analysis in compliance with ISO 9277 [58].  
264 Powdered samples were first preconditioned by outgassing, drying under vacuum at 150 °C for  
265 24 hours [59]. Then their surface areas were analysed using nitrogen absorption/desorption  
266 method [60]. It is worth mentioning that the small amount of samples (around 0.2 g) but higher  
267 volume of nitric acid solution used could minimise the possible neutralisation effect of  
268 powdered samples. This test allows to establish the status or neutralization capacity that each  
269 binder have before being exposed to the acid used in the study, at day 1. It informs on the  
270 potential of the binder disregarding the physical properties or the acid use.

### 271 **3. Results and discussion**

#### 272 **3.1. Basic properties before acid immersion**

273 The basic properties of the three mixes prior to the acid exposure are shown in Table 3. From  
274 Table 3, it is clear that all specimens obtained similar compressive strength ( $62 \pm 3$  MPa) before  
275 immersion. 65Slag\_35OPC and 50Slag\_50FA had the highest and lowest water absorption and  
276 VPV respectively, due to their largest and lowest amount of mixing water used (Table 2)  
277 accordingly. However, 65Slag\_35OPC pastes displayed the lowest capillary sorptivity despite  
278 of its highest water absorption and VPV. This might be explained by considering its porous  
279 structure changes during the 56-day curing period. Due to the largest amount of mixing water  
280 used, many pores were left in the binder matrix after water evaporation, leading to the highest  
281 water absorption and VPV [2]. However, the late hydration process of this paste due to partial  
282 replacement of OPC by slag refined its porous structures [61], leading to the formation of many  
283 isolated pores which reduced the continuity of pore structures. Thus, a low capillary sorptivity  
284 was obtained. As a higher rate of water ingress caused by capillary forces indicates a higher  
285 susceptibility of early-stage acid attacks as water is the vehicle of aggressive ions, it suggests

286 that 50Slag\_50FA and 100OPC are more vulnerable towards acid attacks compared to  
 287 65Slag\_35OPC from the perspective of porous media [2].

288 **Table 3**

289 Basic properties of the paste samples used in this test prior to the immersion in the phosphoric  
 290 acid attack.

Sample ID	Water absorption (%)	VPV (%)	Capillary sorptivity (mm/min <sup>0.5</sup> )	Compressive strength (MPa)
50Slag_50FA	17.7 ± 0.1	29.3 ± 0.2	0.36 ± 0.03	64.33 ± 5.78
65Slag_35OPC	26.6 ± 0.1	38.4 ± 0.1	0.14 ± 0.05	59.90 ± 6.44
100OPC	19.6 ± 0.3	31.3 ± 0.4	0.33 ± 0.01	64.92 ± 3.78

291 VPV-Volume of permeable voids.

## 292 3.2. Degradation kinetics

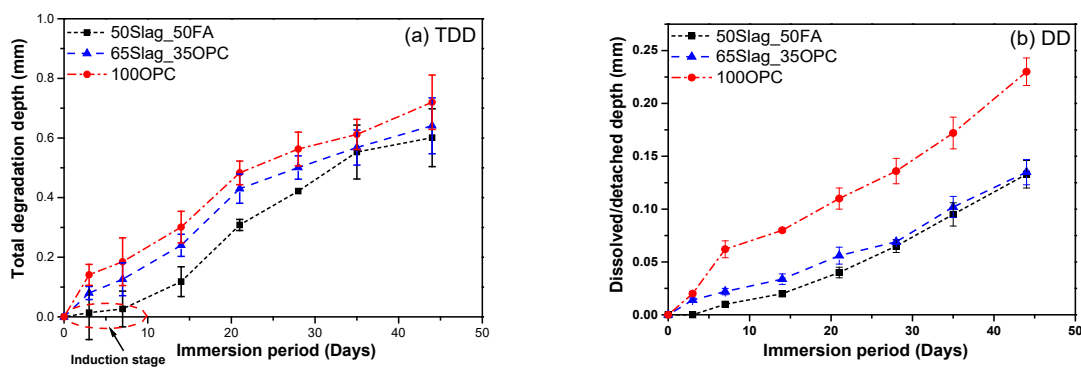
### 293 3.2.1. Degradation depth

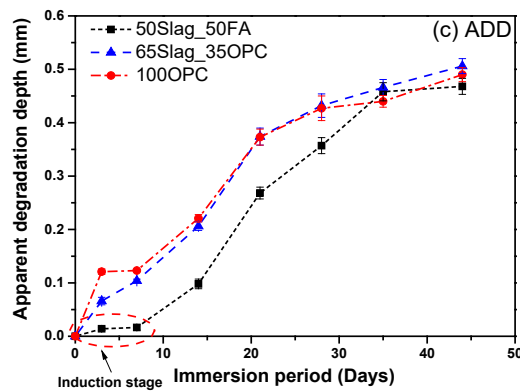
294 The degradation depths, including TDD, DD and ADD of all mixes exposed to the  
 295 phosphoric acid solution within 44 days of immersion are shown in Fig. 3(a)-(c). From Fig.  
 296 3(a), the TDD of 50Slag\_50FA specimen was less than that of the two OPC-based counterparts  
 297 throughout the immersion period, especially within about 0-14 days. Besides, it seems that  
 298 50Slag\_50FA specimen displayed an induction stage within 7 days of immersion with very  
 299 little degradation depth measured as highlighted in a red dash circle. After 7 days, the TDD of  
 300 50Slag\_50FA increased considerably until 35 days followed by a lower rate of increase until  
 301 the end of the 44-day immersion with final TDD at 0.60 mm. In contrast, the 65Slag\_35OPC  
 302 had an almost linear increase in TDD first within 21 days and then the TDD increased at a  
 303 lower rate until the end of exposure. 100OPC followed a similar trend as that of 65Slag\_35OPC  
 304 but with larger TDD throughout the whole immersion period. After 44 days of immersion, the  
 305 TDD of 65Slag\_35OPC and 100OPC was 0.64 and 0.72 mm respectively.

306 For DD values (Fig. 3(b)), 50Slag\_50FA and 65Slag\_35OPC specimens exhibited similar  
 307 trends, increasing almost linearly against immersion period with the DD of 65Slag\_35OPC  
 308 slightly larger. In comparison, 100OPC had a much larger DD over the entire immersion period  
 309 compared to the other two binders. This significant difference can be explained by considering  
 310 the different intrinsic chemical stability of main components in the binder matrix: portlandite  
 311 [Ca(OH)<sub>2</sub>], ettringite and C-S-H gel (the main hydration products in 100OPC binder) can be  
 312 dissolved and/or decomposed completely by acid attacks via decalcification process when pH  
 313 is around 3 or lower regardless of acid types [62]. As C-S-H gel is the main contributor to the  
 314 strength of OPC-based binders [63], accounting for 60%-75% of the total volume of paste [64,

315 65], its dissolution and decomposition can thus result in almost complete disintegration of the  
 316 whole binder matrix (evidenced by the largest DD). However, due to higher contents of Al but  
 317 lower contents of Ca in slag and FA compared to OPC (Table 1), the binding gels formed in  
 318 50Slag\_50FA or 65Slag\_35OPC have more Al and less Ca compared to 100OPC. It is  
 319 confirmed that gels with more Al are more stable and resistant towards decalcification due to  
 320 their more intensely cross-linked networks [66]. Besides, Al and Si have a higher pH stability,  
 321 or greater ability to not leach out of binder at a certain pH, compared to Ca [54]. These explain  
 322 why 50Slag\_50FA and 65Slag\_35OPC obtained much less DD compared to 100OPC.

323 From Fig. 3(c), 50Slag\_50FA had very little ADD within the 7 days of immersion (also  
 324 marked as ‘induction stage’) followed by a significant rise from 7-35 days. 65Slag\_35OPC and  
 325 100OPC samples obtained similar ADD values with a seemingly proportional increase over  
 326 the immersion period. After 44 days, the ADD was 0.47, 0.51 and 0.49 mm for 50Slag\_50FA,  
 327 65Slag\_35OPC and 100OPC respectively. Different ADD are closely associated with available  
 328 OH<sup>-</sup> (hydroxyls) in the binder matrix based on its definition: if the pore solution of binder  
 329 matrix has a high concentration of OH<sup>-</sup> that can neutralise H<sub>3</sub>O<sup>+</sup> from the acid solution, the pH  
 330 of the pore solution can maintain relatively stable for a certain period. However, if the  
 331 concentration of OH<sup>-</sup> is not high enough to neutralise H<sub>3</sub>O<sup>+</sup> or they are neutralised at the  
 332 expense of the formation of many cracks near the sample surface, the pH of the pore solution  
 333 would decrease rapidly. Hence, the delayed ADD evolution of 50Slag\_50FA evidenced by the  
 334 induction stage suggests it has a large reservoir of soluble and mobile alkalis which prevent a  
 335 sudden drop in the pH of AASF pore solutions [67]. In comparison, the instant response of pH  
 336 increment implies that the two OPC pastes either had a lower concentration of OH<sup>-</sup> in the pore  
 337 solution and/or the binder matrix was severely disintegrated, thus providing almost no extra  
 338 ‘protection’ against the acid penetration.



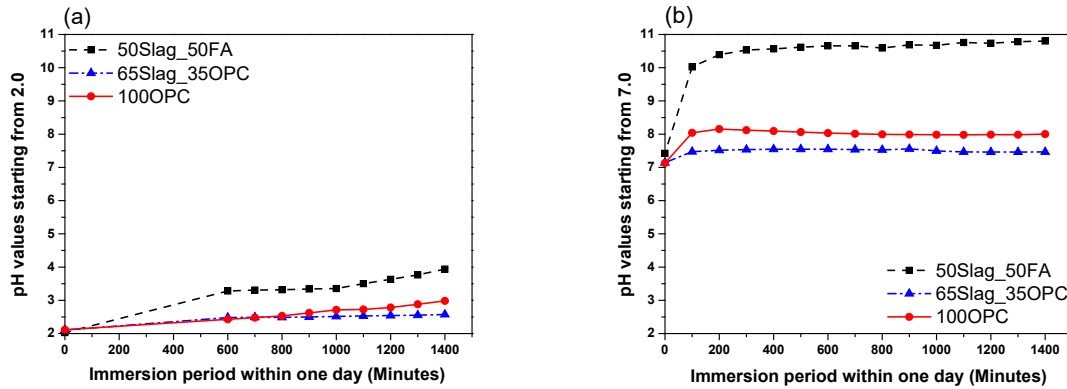


340

341 **Fig. 3.** The (a) TDD, (b) DD and (c) ADD of the three cementitious pastes exposed to the phosphoric  
 342 acid ( $\text{pH} = 2.0 \pm 0.2$ ) over 44-day of immersion.

343 To confirm this, the pH evolutions over the first day of immersion in phosphoric acid and  
 344 water are shown in Fig. 4. It is apparent that 50Slag\_50FA led to a greater increase in the pH  
 345 of the corresponding solutions compared to that of the OPC-based peers both in the phosphoric  
 346 acid and in water, suggesting that it has a stronger neutralisation capacity. Considering the least  
 347 ADD of 50Slag\_50FA, it seems to have an ability to maintain the pH of pore solution at a high  
 348 level ( $\text{pH} > 8.3$ ) because of a large reservoir of  $\text{OH}^-$  that is readily available to neutralise  
 349 external  $\text{H}_3\text{O}^+$  ions. This result corresponds well with the other studies [51, 67] which reported  
 350 that the concentration of  $\text{OH}^-$  in the pore solution of one type AASF with the same slag/FA  
 351 ratio is more than 1000 mmol/L, indicating a pH higher than 14. Besides, bound alkalis provide  
 352 the AAMs with a large reservoir of exchangeable cations to prevent a sharp drop in the pH of  
 353 pore solutions. However, the pH of the pore solutions of OPC binders is relatively lower,  
 354 ranging between 12.5 and 13.5 [68-70] and that's why OPC-based binders had larger ADD  
 355 than that of the 50Slag\_50FA paste. The significant increase in the ADD of 50Slag\_50FA after  
 356 7 days reveals that most of the  $\text{OH}^-$  available were almost consumed. The final slightly larger  
 357 ADD for 65Slag\_35OPC than 100OPC is consistent with the former's smaller increase in the  
 358 pH in Fig. 4(a) and (b). This is because 100OPC has a large amount of Portlandite which is  
 359 able to consume  $\text{H}_3\text{O}^+$ , also known as the buffer effect [71].

360 In conclusion, the 'induction stage' in ADD and TDD is closely associated with the higher  
 361 neutralisation capacity of the 50Slag\_50FA specimen, providing a buffering effect during the  
 362 early stage.



363

364 **Fig. 4.** The pH variations of (a) phosphoric acid solution and (b) water solution within the first day of  
 365 immersion.

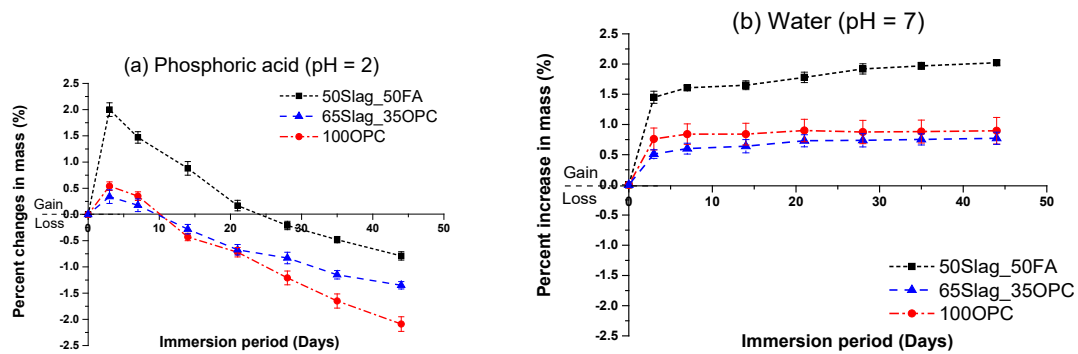
### 366 3.2.2. Mass changes

367 Fig. 5 presents the mass changes of the three binder mixes in the phosphoric acid and in  
 368 water as reference over the early-stage immersion period. The obvious initial mass gain for all  
 369 binder mixes regardless of phosphoric acid solution or water is due to water absorption and  
 370 similar results were also reported in previous studies [72, 73]. After a certain period, mass  
 371 losses were observed for specimens exposed to phosphoric acid whereas a slight mass increase  
 372 or a constant mass was observed for 50Slag\_50FA and OPC-based binders respectively for the  
 373 immersion in water.

374 For immersion in the phosphoric acid, 50Slag\_50FA experienced the largest mass increase  
 375 (2%) after about three days followed by a decrease in mass gain up to about 24 days. After that,  
 376 the actual mass loss occurred with the final mass loss at 0.79% by end of the immersion. The  
 377 largest mass increase for 65Slag\_35OPC and 100OPC sample was 0.34% and 0.54%  
 378 respectively after 3-day immersion, much smaller than that of the 50Slag\_50FA. An apparent  
 379 mass loss compared to the initial value was observed after about 10 days for the two OPC-  
 380 based mixes, about 14 days earlier compared to the 50Slag\_50FA. The highest mass gain and  
 381 delayed mass loss for the 50Slag\_50FA might be associated with its highest capillary sorptivity  
 382 (Table 3), relatively stability of binding components and possible precipitations of some  
 383 reaction products. For 65Slag\_35OPC sample, the mass loss decelerated gradually whereas the  
 384 mass loss decreased almost constantly for 100OPC. The final mass loss of the two was 1.35%  
 385 (65Slag\_35OPC) and 2.09% (100OPC).

386 In conclusion, the mass losses of the three mixes were consistent with the degradation  
 387 depths, with an increasing order at 50Slag\_50FA < 65Slag\_35OPC < 100OPC. It is worth  
 388 noting that the much greater mass gain owing to acid solution ingress for the 50Slag\_50FA but

389 similar starting point of the loss in mass gain at about 3 days for all mixes suggest that this  
 390 binder is more resistant towards mass losses due to this acid attack compared to the OPC-based  
 391 peers. It is suggested to use fully-saturated specimens before immersion in acid solutions to  
 392 avoid misleading mass gains caused by the ingress of acid solutions.



393  
 394 **Fig. 5.** Mass changes over 44-day immersion time for the three binder mixes in (a) phosphoric acid  
 395 and (b) water.

### 396 3.2.3. Leaching rates of related elements

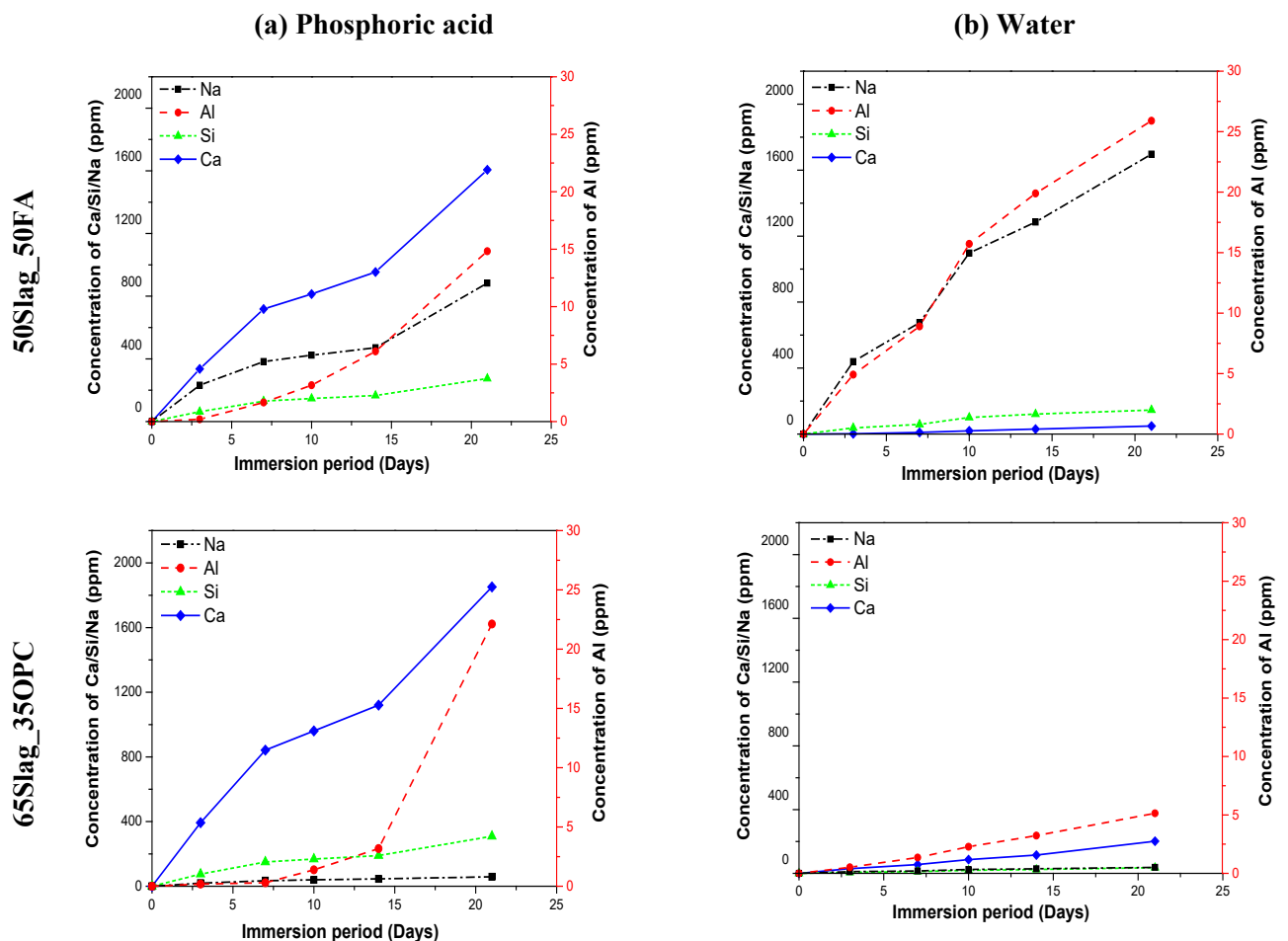
397 The leaching behaviour the related elements released from the three mixes during 21 days  
 398 of immersion in the phosphoric acid and in water are depicted in Fig. 6. The cumulative  
 399 concentration of Na, Ca, Al and Si is denoted as [Na], [Ca], [Al] and [Si] respectively hereafter.  
 400 Due to insignificant contents of Na in the OPC-based binders, [Na] is not discussed for OPC-  
 401 based binders.

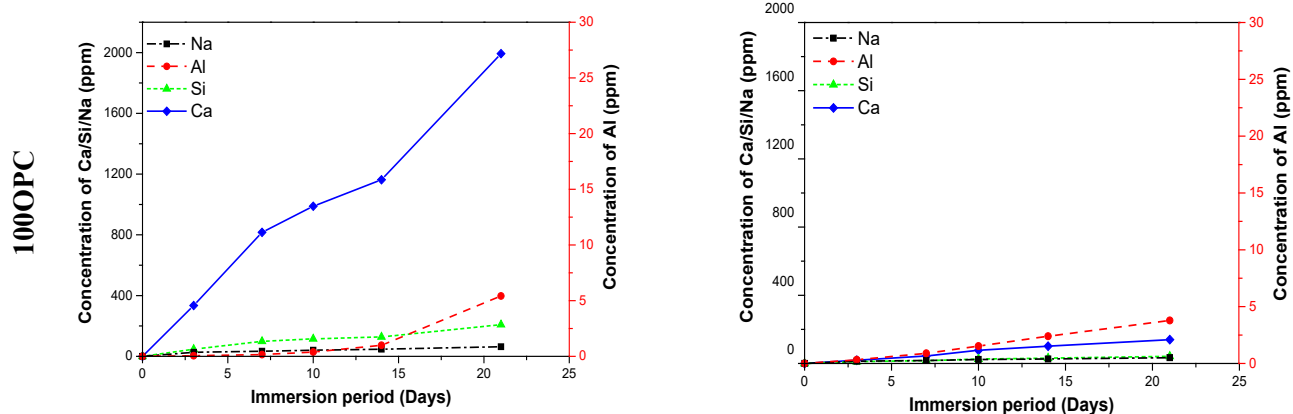
402 During immersion in the phosphoric acid, a remarkable increase in [Ca] can be observed for  
 403 all mixes compared to the [Si], [Al] or [Na]. For instance, the [Ca] was 1606.6 ppm for the  
 404 solution containing 50Slag\_50FA, which was even higher than the total sum of [Si], [Al] and  
 405 [Na] (1172.7 ppm). This phenomenon is attributed to the high content of Ca in all mixes and  
 406 higher neutralisation capacity of bivalent  $\text{Ca}^{2+}$  ions compared to monovalent  $\text{Na}^+$ .  
 407 50Slag\_50FA also led to a large [Na] which was 883.4 ppm owing to the sodium-based alkaline  
 408 activator used while making the specimen. The high [Ca] and [Na] are in line with the highest  
 409 neutralisation capacity and the presence of 'induction stage' for 50Slag\_50FA because these  
 410 counter-balancing ions are accompanied with a lot of  $\text{OH}^-$ , maintaining the pH value of the  
 411 pore solution for a while without considerably affecting the stability of the binding phase. The  
 412 [Al] and [Si] for 50Slag\_50FA were much lower, which was 14.8 ppm and 274.5 ppm  
 413 respectively. Similarly, the corresponding value was 22.1 and 309.0 ppm for 65Slag\_35OPC,  
 414 5.4 and 208.5 ppm for 100OPC respectively. All of these suggest that Al and Si are less  
 415 sensitive compared to Ca when exposed to the acid attack [54]. It is worth noting that for all

416 mixes, the release of Al seemed to be curbed probably because of the relative high stability of  
 417 Al-bearing phases, such as C-(N)-A-S-H in the 50Slag\_50FA and calcium aluminate phases in  
 418 OPC-based binders [19, 74].

419 Compared to the [Ca] in the phosphoric acid, [Ca] in water was much lower irrespective of  
 420 binder mixes indicating that Ca is quite sensitive to  $H_3O^+$  induced by the acid solution. In  
 421 addition, the [Na] and [Al] in water for 50Slag\_50FA was higher due to their high mobility,  
 422 especially for Na. The OPC-based two mixed binders had similar [Al] and [Si] which increased  
 423 almost linearly with an increase in the immersion periods.

424 In summary, Ca is much more sensitive towards  $H_3O^+$  compared to Si and Al, corresponding  
 425 well with the results from other research [75, 76]. Moreover, apart from Ca, 50Slag\_50FA can  
 426 release a large amount of Na which plays an important role in consuming  $H_3O^+$  ions produced  
 427 by acid solutions and maintaining a stable pH of the pore solution.





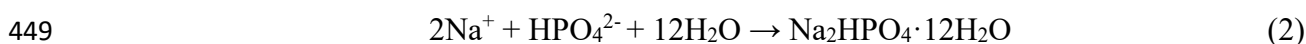
428  
 429 **Fig. 6.** Cumulative concentrations of different elements in the two solutions released from the three  
 430 mixes within 21 days of immersion, (a) Phosphoric acid; (b) Water.

431 **3.3. Microstructural characterisation**

432 **3.3.1. Mineralogy**

433 *X-ray diffraction (XRD)*

434 Fig. 7 shows the XRD spectra of the three mixes after 44 days of immersion in the phosphoric  
 435 acid solution. Based on Fig. 7(a), it can be seen that due to the acid attack, major components  
 436 such as Ca-bearing gismondine ( $\text{CaO} \cdot \text{Al}_2\text{O}_3 \cdot 2\text{SiO}_2 \cdot 4\text{H}_2\text{O}$  PDF # 00-002-0096) and C-(N)-(A)-  
 437 S-H (a type of calcium silicate hydrate substituted by Al and Na) [39, 77-79] which are present  
 438 in the undegraded part of 50Slag\_50FA all disappear. Quartz (PDF # 00-001-0649) and mullite  
 439 (PDF # 00-001-0613), however, still appear due to some unreacted FA in the degraded part.  
 440 This result implies that the phosphoric acid attack resulted in decalcification of the main  
 441 binding gels in the 50Slag\_50FA paste along with dealkalisation and dealumination. The  
 442 dealkalisation and dealumination were also verified by the leaching results of Al and Na in Fig.  
 443 6. Moreover, some phosphates were identified in the degraded part, such as Brushite  
 444 ( $\text{CaHPO}_4 \cdot 2\text{H}_2\text{O}$  PDF # 00-001-0395) and sodium phosphate hydrate oxide ( $\text{Na}_2\text{HPO}_4 \cdot 12\text{H}_2\text{O}$   
 445 PDF # 00-001-0223). The formation of Brushite was also reported in another study [1] due to  
 446 silage effluent attacks as silage effluents also contain phosphates. Possible chemical reactions  
 447 are shown below:

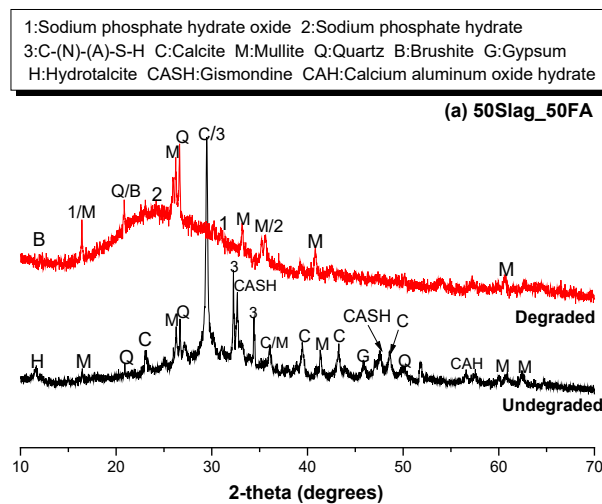


450 Fig. 7(b) and (c) shows that Portlandite ( $\text{Ca}(\text{OH})_2$  PDF # 00-001-1079), C-S-H gel (PDF #  
 451 00-002-0068), calcite ( $\text{CaCO}_3$  PDF # 00-001-0837) and ettringite ( $\text{Ca}_6\text{Al}_2(\text{SO}_4)_3(\text{OH})_{12} \cdot 26\text{H}_2\text{O}$   
 452 PDF # 00-002-0059) are main phases in the OPC-based binding matrix without acid attacks.

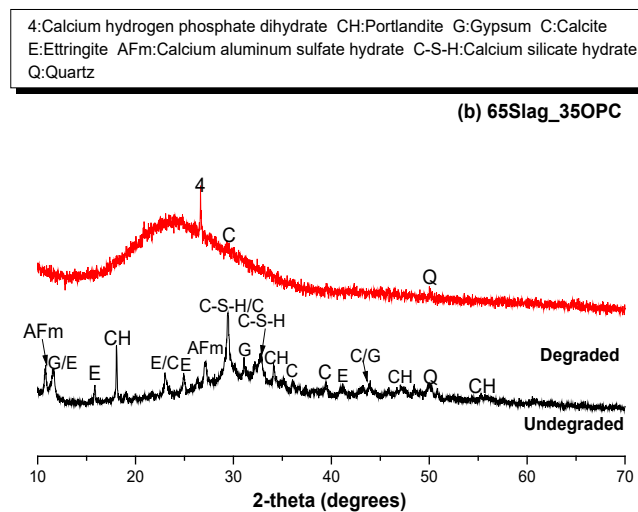
453 However, all of these phases disappear in the corresponding degraded parts, indicating their  
 454 vulnerability to the phosphoric acid [74]. For 65Slag\_35OPC, minor traces of quartz (PDF #  
 455 00-001-0649) and calcium hydrogen phosphate dihydrate (CaHPO<sub>4</sub>·2H<sub>2</sub>O PDF # 00-001-0653)  
 456 were detected in the degraded part. Brushite (CaHPO<sub>4</sub>·2H<sub>2</sub>O PDF # 00-001-0395) and a type  
 457 of calcium phosphate hydrate (Ca(H<sub>2</sub>PO<sub>4</sub>)<sub>2</sub>·H<sub>2</sub>O PDF # 00-001-0471) can be observed in the  
 458 degraded part of 100OPC binder. The presence of the Ca(H<sub>2</sub>PO<sub>4</sub>)<sub>2</sub>·H<sub>2</sub>O can be explained by  
 459 the reaction below that could happen in the interstitial solution or at the surface of the sample:



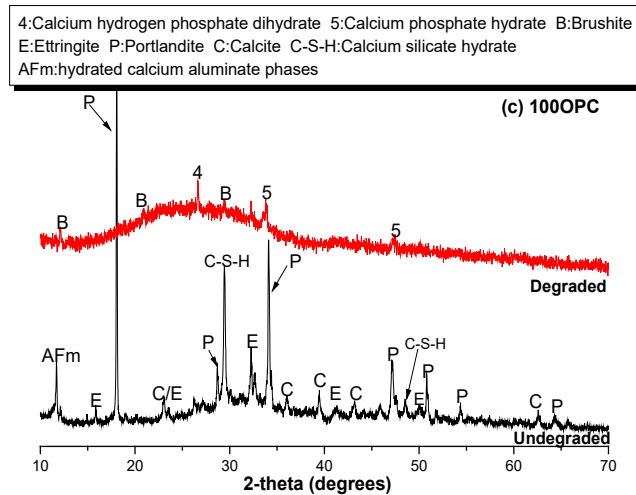
461 It is also noticed that after the phosphoric acid immersion, a wide halo is present in degraded  
 462 parts of all mixes (extending from around 15 to about 35° 2θ). These can be ascribed to the  
 463 formation of amorphous phases due to acid attacks [19]. The wider and more flattened halo of  
 464 100OPC sample than the other two binders indicates a more severely degraded part, consistent  
 465 with the highest degradation kinetic of 100OPC.



466



467



468

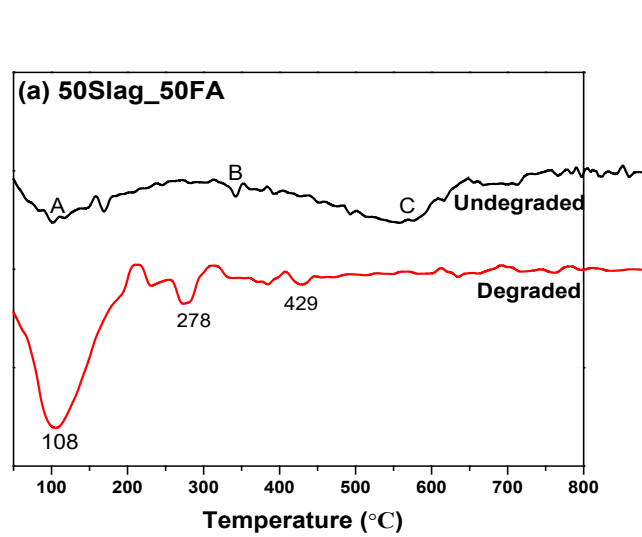
469 **Fig. 7.** XRD patterns of the three mixture pastes (a) 50Slag\_50FA; (b) 65Slag\_35OPC and (c)  
 470 100OPC including both degraded and undegraded parts after 44-day immersion period in the  
 471 phosphoric acid ( $\text{pH} = 2.0 \pm 0.2$ ).

472 **Differential Thermogravimetry (DTG)**

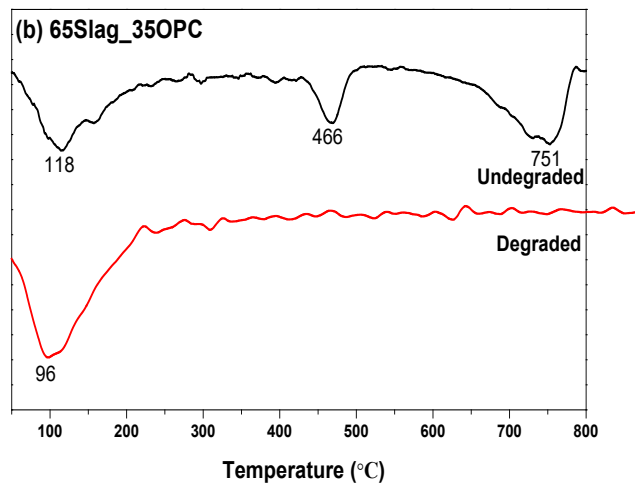
473 DTG curves of the three binder mixes including degraded and undegraded part of specimens  
 474 are shown in Fig. 8. Table 4 lists the characteristic peak attributions for all the curves. It can be  
 475 observed that there are three small peaks marked as 'A', 'B' and 'C', belonging to evaporable  
 476 water or moisture loss from 50Slag\_50FA undegraded binding matrix [80-82], decomposition  
 477 of C-A-S-H and C-A-H [83-85] and decomposition of carbonates (e.g. calcite) [86, 87],  
 478 respectively. In comparison, no 'B' and 'C' peaks could be observed in the degraded part.  
 479 Rather, two obvious peaks located at 278 and 429 °C are present which might be associated  
 480 with the formation of calcium phosphates, as verified in XRD patterns. Besides, a significant  
 481 mass loss exists at around 108 °C, indicating that more water (loosely bound or unbound) is  
 482 evaporable after the acid attack due to the transformation of many original crystalline phases  
 483 to amorphous ones, as shown in Fig. 7(a).

484 For the undegraded part of the OPC-based binders, the first mass occurring at 118 °C and  
 485 117 °C respectively for 65Slag\_35OPC and 100OPC can be assigned to the loss of evaporable  
 486 free water, dehydration of C-S-H gel and ettringite [80, 81, 88]. The peaks centered at 466 and  
 487 467 °C for 65Slag\_35OPC and 100OPC respectively are due to the dehydroxylation of  
 488 Portlandite [81]. The last significant mass loss located at around 750 or 751 °C is attributed to  
 489 the decomposition of carbonate minerals, such as calcite [89, 90], in accordance with the XRD  
 490 results. Similar to XRD, corresponding peaks assigned to Portlandite and calcites are not  
 491 present in the DTG curves of the degraded part. The only obvious mass loss located at lower  
 492 temperatures, 96 °C (65Slag\_35OPC) and 94 °C (100OPC), compared to those in the

493 undegraded part, indicates the presence of a larger amount of less tightly bound water. This is  
494 in large part due to the formation of some less crystalline and amorphous phases such as silica-  
495 gel after the phosphoric acid immersion, corresponding well with the wide halo in the XRD  
496 results. It is noteworthy that no phosphates are noticeable in OPC-based DTG curves, probably  
497 because the total amount of these phosphates are too small to be detected or most of them were  
498 dissolved in the acid solution. Based on the XRD results which show traces of calcium  
499 phosphates, it is highly possible only a little amount phosphates were left in the degraded layer  
500 of OPC binders.

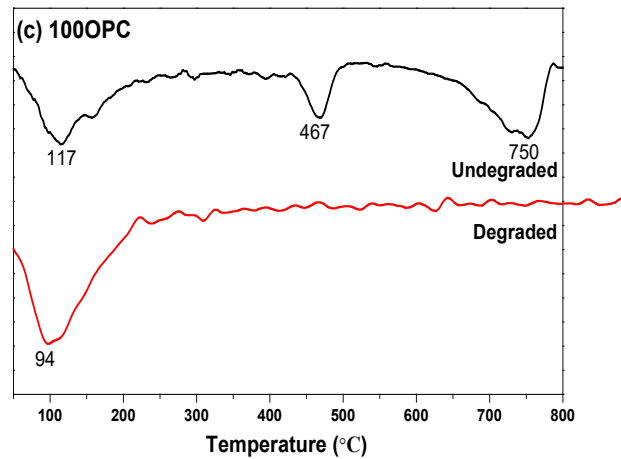


501



502

503



504

505 **Fig. 8.** DTG curves of the three mixes including degraded and undegraded part of the specimen.

506 **Table 4**

507 Temperature ranges within or at which corresponding changes in phases take place.

Different phases and changes	Temperature ranges (°C)	References
Loss of evaporable water	0–120, usually < 100	[80, 81]
Removal of the moisture within C-S-H type gel	50-200	[91, 92]
Loss of water in N-A-S-H	≈ 100	[82]
Loss of bound water in C-(A)-S-H	30-650	[91]
Decomposition of ettringite	114-116/110-170/104-114	[93, 94]/[81]/[95]
Mass loss of AFm phases	146	[96-99]
Dehydroxylation of calcium hydroxide	450-550/430-520	[81, 95, 100]/[86]
Decomposition of carbonates	560-700/741-797	[86, 87]/[89, 90]

508

### 509 3.3.2. Microstructure

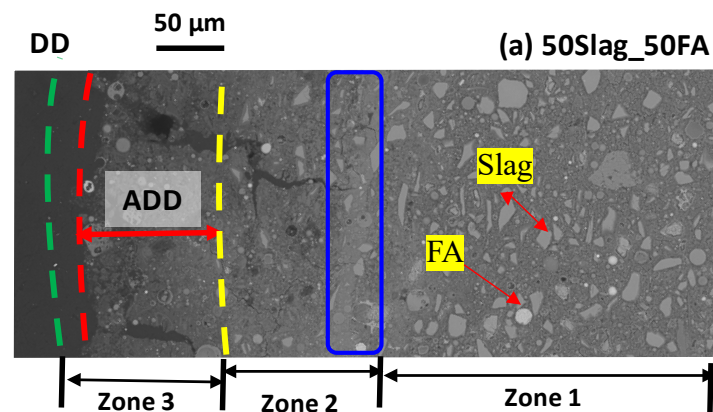
#### 510 *ESEM and EDS*

511 SEM images in backscattering mode and elemental distributions of the three mixes after 14  
 512 days of immersion are shown in Fig. 9 and Fig. 10 respectively. The corresponding DD and  
 513 ADD obtained from Fig. 3 are also marked. The DD of the 50Slag\_50FA, 65Slag\_35OPC and

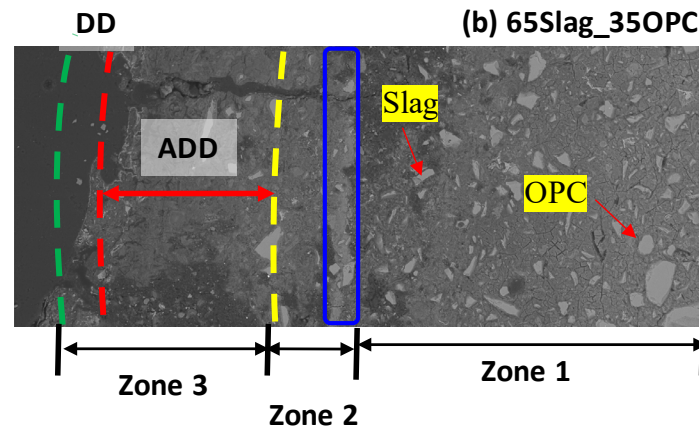
514 100OPC was 20.0, 33.8 and 80.0  $\mu\text{m}$  respectively and the corresponding ADD was 96.6, 206.2  
515 and 188.4  $\mu\text{m}$  respectively.

516 In Fig. 9, it is clear that three zones can be identified for all the samples: Zone 1 represents  
517 the undegraded part of the samples with brighter grey colour compared to other regions as it  
518 contains many unhydrated OPC particles for OPC-based binders or unreacted slag and FA  
519 particles for 50Slag\_50FA [72, 101]. Zone 2 is a transition zone starting from a bright grey  
520 narrow strip (partitioned as blue solid line frames) which should be a region rich in phosphates  
521 (as discussed later) to the right boundary of ADD (yellow dashed line, also considered as the  
522 ‘reaction front’). In this zone, both obvious cracks (closer to surface) and unreacted/unhydrated  
523 particles exist. Zone 3 is composed of DD and ADD with many microcracks and voids,  
524 indicating a severe degradation result.

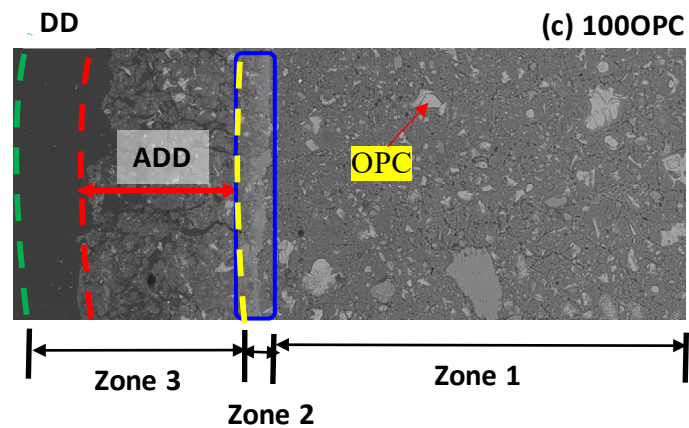
525 The most distinct part is Zone 2 of 50Slag\_50FA compared to that of the other OPC-based  
526 pastes. Firstly, the width of the narrow strip is apparently larger indicating more precipitations  
527 of phosphates, in accordance with the mineralogical analysis (shown in Fig. 8(a)). Additionally,  
528 50Slag\_50FA has a thicker Zone 2, implying a stronger resistance to the ingress of  $\text{H}_3\text{O}^+$  ions  
529 as they need to penetrate this zone first before attacking new undegraded areas. This is critical  
530 for maintaining high resistance towards acid attacks. This thicker zone 2 has also been reported  
531 in previous studies [19, 102].



532



533



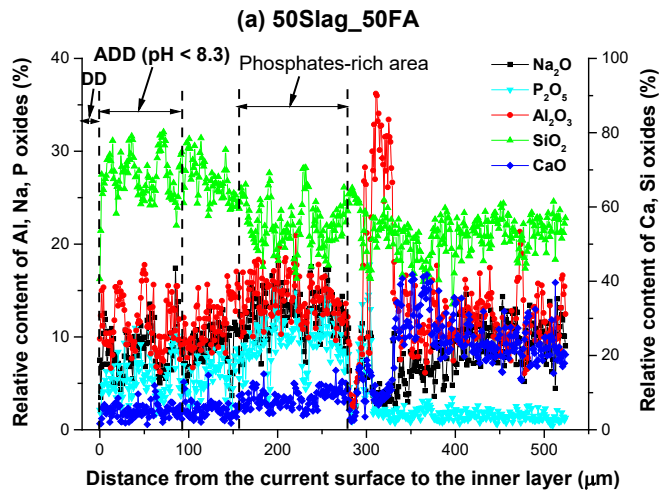
534

535 **Fig. 9.** SEM images of the paste samples (a) 50Slag\_50FA; (b) 65Slag\_35OPC and (c) 100OPC after  
 536 14 days of immersion in the phosphoric acid.

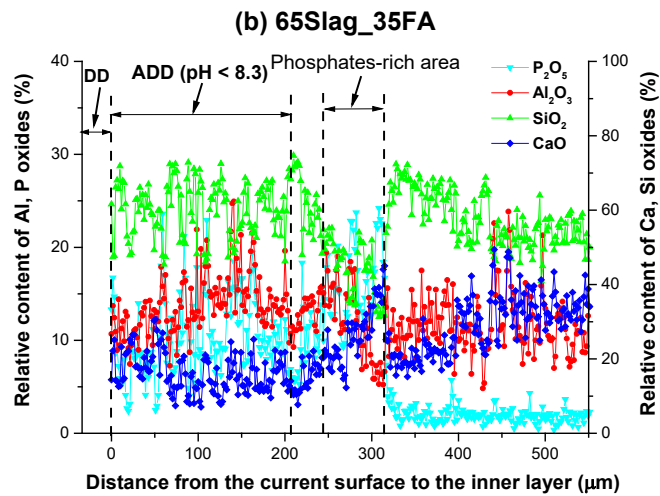
537 The elemental distributions from the surface to the inner part of the specimens are shown in  
 538 Fig. 10. Consistent with the locations of the blue solid line frames in Fig. 9, a much higher  
 539 phosphorus concentration is observable implying the precipitations of different phosphates. A  
 540 closer examination shows that the phosphates-rich area of 50Slag\_50FA is located farther from  
 541 the reaction front followed by that of 65Slag\_35OPC and 100OPC. For all mixes, the relative  
 542 concentration of Ca decreased as approaching to the degraded surface while Al and Si  
 543 displayed the opposite trend, in agreement with the previously noted leaching behaviour of  
 544 these elements. Even if the solid/liquid ratio in the leaching test was lower, it still demonstrates  
 545 that Ca is more sensitive towards acid attacks compared to Al and Si.

546 50Slag\_50FA encountered an increase in the relative concentration of Al accompanied with  
 547 a decrease in the Ca and Na relative content. This can be explained by the ease of ion exchanges  
 548 of Ca and Na with  $H_3O^+$  compared to Al, in line with the delayed leaching behaviour of Al  
 549 noted in the leaching test even at lower solid/liquid ratio and as shown in the ICP-OES analysis  
 550 and other studies [103]. It seems that Al is much less mobile in AAM binding gels because

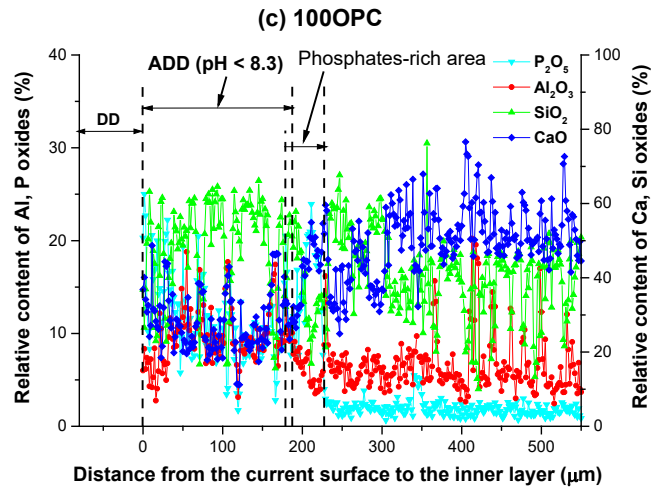
551 according the previous studies, more Al are in coordinate 3 ( $q^3$ ) than in coordinate 2 ( $q^2$ ) [104,  
 552 105] in these systems, giving them a better stability toward acids compared to Na and Ca [106].  
 553 The higher concentrations of Al and Si also confirms an aluminosilicate type gel formed in the  
 554 degraded area. In contrast, OPC-based pastes had no such sharp increase in the relative  
 555 concentration of Al and the changes of Ca or Al were relatively stable.



556



557



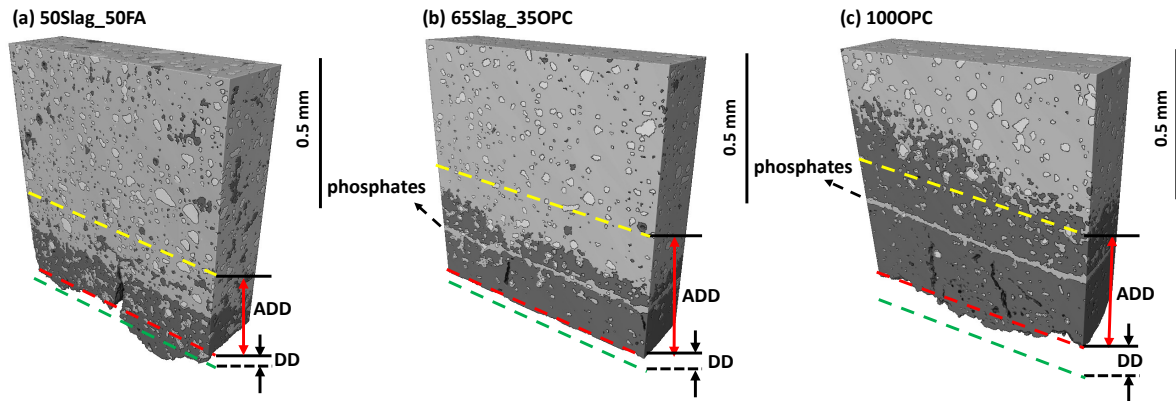
558

559 **Fig. 10.** Chemical analysis of different elements relative content measured by EDS line scan after 14  
 560 days of immersion in the phosphoric acid, (a) 50Slag\_50FA; (b) 65Slag\_35OPC and (c) 100OPC.

561 **Micro-CT analysis**

562 Three dimensional images of the three mixes after 21 days of acid immersion are shown in  
 563 Fig. 11 and corresponding ADD and DD values based on Fig. 3 are also provided. Similar to  
 564 SEM images, light-grey areas refer to undegraded components with fewer pores and more  
 565 unreacted particles (higher density) whereas darker grey areas represent phases containing  
 566 more pores and fewer unreacted particles (lower density) meaning they are already partially or  
 567 completely degraded. The resolution was 1.78 μm in this study.

568 For 50Slag\_50FA and 65Slag\_35OPC samples, it is apparent that the binders remain more  
 569 or less undegraded (light grey) even when the pH is lower than 8.3 (within the ‘ADD’ area),  
 570 which is not the case for 100OPC. Oppositely, the 100 OPC sample displayed some degraded  
 571 parts where the pH is still above 8.3 (outside of ‘ADD’ area). This result is in consistent with  
 572 the pH stability of different components in the corresponding binders. For 100OPC, the main  
 573 components including Ca(OH)<sub>2</sub>, ettringite and C-S-H all disappear when pH is lower than 10.5  
 574 and thus degraded part is present even when pH is still above 8.3 [26]. In comparison, less  
 575 soluble and mechanically sound aluminosilicate gel even after exposure to acids with pH at 3  
 576 [27, 107] in 50Slag\_50FA and 65Slag\_35OPC (also rich in C-(A)-S-H) explains why phases  
 577 within ‘ADD’ were still stable. A light grey layer can be observed in the degraded part of the  
 578 two OPC-based binders, which is assumed to be different phosphates.



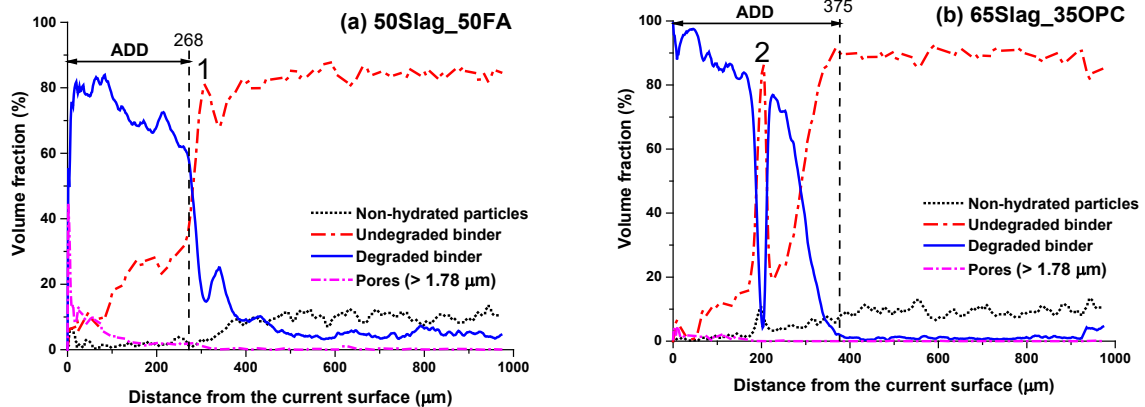
579

580 **Fig. 11.** 3D micro-CT images of the samples after 21-day exposure towards the phosphoric acid: (a)  
 581 50Slag\_50FA; (b) 65Slag\_35OPC and (c) 100OPC. DD and ADD are also labelled based on the  
 582 experimental results. Green dashed lines refer to the original surfaces of pastes.

583

584 Different volume fractions of the phases in the corresponding mixes based on the 3D images  
 585 after segmentation and data processing procedure are presented in Fig. 12. The four types of  
 586 components are determined based on their different relative densities obtained from Fig. 11.  
 587 ADD values are also included to correlate different components with pH values of pores. The  
 588 number '1', '2' and '3' indicate the main location of the precipitated phosphates because the  
 589 undegraded binder experienced an abrupt increase in volume fraction as approaching to the  
 590 surface which is assumed to be the phosphates with a higher density than the degraded binder.  
 591 It is also apparent that the undegraded binder maintained a certain volume even within the  
 592 'ADD' region.

593



594

595

596

597

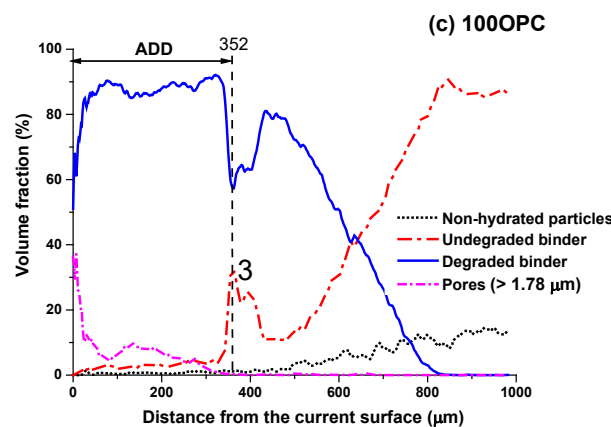
598

599

600

601

602



603

604

605

606 **Fig. 12.** Volume fractions of different components in three mixes after 21 days of immersion for (a)  
607 50Slag\_50FA, (b) 65Slag\_35OPC and (c) 100OPC obtained from the current surface of the sample  
608 derived from micro-CT analysis. The ADD values are obtained from Fig. 3.

### 609 **3.4. Dissolution rate of powdered samples**

610 The results of Dissolution Rate (DR) and Normalized Dissolution Rate (NDR) are listed in  
611 Table 5. It is found that 100OPC got the largest NDR ( $0.087 \text{ g/m}^2$ ) followed by 65Slag\_35FA  
612 ( $0.046 \text{ g/m}^2$ ) and 50Slag\_50FA ( $0.041 \text{ g/m}^2$ ). Based on the previous dissolved depth (DD) as  
613 shown in Fig. 3(b), NDR and DD are consistent with each other: compared to the much larger  
614 NDR and DD for 100OPC, the two values for 65Slag\_35FA and 50Slag\_50FA are close with  
615 each other. The only difference is the immersion condition, one is powdered samples exposed  
616 to nitric acid and another one is cylindrical bulk samples immersed in the phosphoric acid.  
617 Therefore, the consistent results imply that both NDR and DD can be used to reflect the  
618 intrinsic chemical resistance of different binders having no influence of the following two  
619 factors: one is porous media in bulk samples (e.g. tortuosity and connectivity) [108, 109] and  
620 another is precipitations of various salts that may further block the surface or inner pores of  
621 samples, leading to some changes in degradation processes [110]. Similar to DD, the NDR of  
622 different binders reflects the intrinsic stability of various binding gels which is also likely due  
623 to the different Al and Ca contents: a higher aluminium but lower calcium content leads to a  
624 lower NDR.

625 **Table 5**

626 Detailed information on the dissolution rate test (48 hours of immersion for different powder  
627 mixes in the nitric acid solution).

Sample ID	Averaged $M_{\text{before}}$ (g)	Averaged $M_{\text{after}}$ (g)	$S$ ( $\text{m}^2/\text{g}$ )	DR	NDR ( $\text{g}/\text{m}^2$ )
50Slag_50FA	0.2002	0.0940	13.07	0.53	0.041
65Slag_35FA	0.1998	0.0058	20.90	0.97	0.046
100OPC	0.2000	0.0195	10.39	0.90	0.087

628 Note:  $M_{\text{before}}$ -the mass of the powdered sample before exposure,  $M_{\text{after}}$ -the mass of the  
629 powdered sample after exposure, S-BET surface area, DR-Dissolution rate, NDR-Normalized  
630 dissolution rate.

#### 631 **4. Conclusions**

632 This study demonstrates the early-stage behaviour of a type of AASF and two types of OPC-  
633 based binders exposed to phosphoric acid ( $\text{pH} = 2$ ) in terms of their degradation kinetics and  
634 related microstructural and mineralogical changes. A higher degradation rate was observed in  
635 the OPC-based binders, especially the 100OPC specimens. The AASF binder with Slag/FA at  
636 1:1 exhibited an 'induction stage' within about 7-day degradation depth evolution, which is  
637 attributed to its higher neutralisation capacity. Using the leaching data, the calcium content in  
638 the binder composition is the most sensitive component of the binder towards acid attack  
639 whereas other elements as Al and Si seem relatively stable or negligibly affected. Hence,  
640 alternative binders, as here AASF, with a higher content of Al and Si displayed stronger  
641 resistance against the phosphoric acid, compared to the 100OPC. The stable highly crosslinking  
642 C-(A)-S-H, in the AASF led to the formation of a thicker transition zone which is beneficial  
643 for resisting further acid migration and also provides a solid space for the precipitation of  
644 different salts such as Brushite. In comparison, 100OPC binder had almost no transition zone  
645 and the main components were already partially degraded even when the pH was still higher  
646 than 8.3 due to a much higher calcium content introduced by OPC in the binding matrix. The  
647 calcium is released at the expense of losing structural integrity, facilitating more ingress of  
648 hydronium ions.

649 65Slag\_35OPC seemed to present an intermediate behaviour between 50Slag\_50FA and  
650 100OPC pastes: it had the largest ADD value due to its lowest neutralisation capacity, similar  
651 to that of the 100OPC. However, it displayed a transition zone because of a relatively lower Ca  
652 content and higher content of Al and Si, leading to a similar DD as that of the 50Slag\_50FA  
653 binder. Thus, it can be considered as an acceptable alternative to pure OPC binders.

654 Considering the initial highest capillary sorptivity of 50Slag\_50FA and highest water  
655 absorption as well as VPV of 65Slag\_35OPC prior to the acid immersion, it is concluded that  
656 the chemistry and structure of the gel formed in each cement has significantly more influence  
657 than their microstructural properties in determining the early-stage degradation performance.

658

## 659 **Acknowledgements**

660 The authors deliver great thanks to Chinese Scholarship Council (CSC), the Geopolymer  
661 and Minerals Processing Group laboratory in the University of Melbourne for financial and  
662 infrastructure support. The Materials Characterisation and Fabrication Platform, at the  
663 University of Melbourne for the XRD analyses and the Bio21 Advanced Microscopy Facilities  
664 for the SEM analyses. This study was also supported by Mrs Laura Jukes who provided great  
665 help during the experimental parts. Thank you for the ARC Research Hub for Nanoscience-  
666 based Construction Material Manufacturing (IH150100006) for financial support.

## 667 **References**

- 668 [1] T.A. Aiken, W. Sha, J. Kwasny, M.N. Soutsos, Resistance of geopolymer and Portland cement based  
669 systems to silage effluent attack, *Cement and Concrete Research* 92 (2017) 56-65.
- 670 [2] S. Pavía, E. Condren, Study of the durability of OPC versus GGBS concrete on exposure to silage  
671 effluent, *Journal of materials in civil engineering* 20(4) (2008) 313-320.
- 672 [3] M.G.D. Gutiérrez-Padilla, A. Bielefeldt, S. Ovtchinnikov, M. Hernandez, J. Silverstein, Biogenic  
673 sulfuric acid attack on different types of commercially produced concrete sewer pipes, *Cement and  
674 Concrete Research* 40(2) (2010) 293-301.
- 675 [4] A. Parande, P. Ramsamy, S. Ethirajan, C. Rao, N. Palanisamy, Deterioration of reinforced concrete  
676 in sewer environments, *Proceedings of the Institution of Civil Engineers-Municipal Engineer*, Thomas  
677 Telford Ltd, 2006, pp. 11-20.
- 678 [5] L. Zhang, P. De Schryver, B. De Gusseme, W. De Muyndck, N. Boon, W. Verstraete, Chemical and  
679 biological technologies for hydrogen sulfide emission control in sewer systems: a review, *Water  
680 research* 42(1-2) (2008) 1-12.
- 681 [6] J. Ren, L. Zhang, R.S. Nicolas, Degradation of Alkali-Activated Slag and Fly Ash Mortars under  
682 Different Aggressive Acid Conditions, *Journal of Materials in Civil Engineering* 33(7) (2021).
- 683 [7] K. Scrivener, N. De Belie, Bacteriogenic sulfuric acid attack of cementitious materials in sewage  
684 systems, *Performance of cement-based materials in aggressive aqueous environments*, Springer2013,  
685 pp. 305-318.
- 686 [8] J. Ren, L. Zhang, R. San Nicolas, Degradation process of alkali-activated slag/fly ash and Portland  
687 cement-based pastes exposed to phosphoric acid, *Construction and Building Materials* 232 (2020)  
688 117209.
- 689 [9] Y. Xie, X. Lin, T. Ji, Y. Liang, W.J.C. Pan, B. Materials, Comparison of corrosion resistance mechanism  
690 between ordinary Portland concrete and alkali-activated concrete subjected to biogenic sulfuric acid  
691 attack, 228 (2019) 117071.
- 692 [10] H.B. Chang, Y.C.J.J.o.M.R. Choi, Technology, Accelerated performance evaluation of repair  
693 mortars for concrete sewer pipes subjected to sulfuric acid attack, 9(6) (2020) 13635-13645.
- 694 [11] A. Özcan, M.B.J.I.J.o.C.E. Karakoç, The resistance of blast furnace slag-and ferrochrome slag-based  
695 geopolymer concrete against acid attack, 17(10) (2019) 1571-1583.
- 696 [12] M. Vafaei, A. Allahverdi, P. Dong, N.J.C. Bassim, B. Materials, Acid attack on geopolymer cement  
697 mortar based on waste-glass powder and calcium aluminate cement at mild concentration, 193 (2018)  
698 363-372.
- 699 [13] P. Sturm, G. Gluth, C. Jäger, H. Brouwers, H.-C.J.C. Kühne, C. Research, Sulfuric acid resistance of  
700 one-part alkali-activated mortars, 109 (2018) 54-63.
- 701 [14] H.A. Khan, A. Castel, M.S. Khan, A.H.J.C. Mahmood, C. research, Durability of calcium aluminate  
702 and sulphate resistant Portland cement based mortars in aggressive sewer environment and sulphuric  
703 acid, 124 (2019) 105852.

704 [15] A. Bertron, J. Duchesne, G. Escadeillas, Degradation of cement pastes by organic acids, *Materials*  
705 *and structures* 40(3) (2007) 341-354.

706 [16] S. Larreur-Cayol, A. Bertron, G. Escadeillas, Degradation of cement-based materials by various  
707 organic acids in agro-industrial waste-waters, *Cement and Concrete Research* 41(8) (2011) 882-892.

708 [17] O. Oueslati, J. Duchesne, The effect of SCMs and curing time on resistance of mortars subjected  
709 to organic acids, *Cement and Concrete Research* 42(1) (2012) 205-214.

710 [18] M. Alexander, C. Fourie, Performance of sewer pipe concrete mixtures with portland and calcium  
711 aluminate cements subject to mineral and biogenic acid attack, *Materials and structures* 44(1) (2011)  
712 313-330.

713 [19] T. Gutberlet, H. Hilbig, R.E. Beddoe, Acid attack on hydrated cement — Effect of mineral acids on  
714 the degradation process, *Cement and Concrete Research* 74 (2015) 35-43.

715 [20] E. Galanos, K. Gray, A. Biddlestone, K. Thayanithy, The aerobic treatment of silage effluent:  
716 effluent characterization and fermentation, *Journal of agricultural engineering research* 62(4) (1995)  
717 271-279.

718 [21] M.M. Gebrehanna, R.J. Gordon, A. Madani, A.C. VanderZaag, J.D. Wood, Silage effluent  
719 management: A review, *Journal of Environmental Management* 143 (2014) 113-122.

720 [22] J. Ren, S. Guo, J. Su, T. Zhao, J. Chen, S. Zhang, A novel TiO<sub>2</sub>/Epoxy resin composited geopolymer  
721 with great durability in wetting-drying and phosphoric acid solution, *Journal of Cleaner Production*  
722 227 (2019) 849-860.

723 [23] M. Secco, G.I. Lampronti, M.-C. Schlegel, L. Maritan, F. Zorzi, Degradation processes of reinforced  
724 concretes by combined sulfate–phosphate attack, *Cement and Concrete Research* 68 (2015) 49-63.

725 [24] J. Ren, L. Zhang, R. San Nicolas, Degradation of alkali-activated slag/fly ash mortars under different  
726 aggressive acid conditions, *Journal of materials in civil engineering* (2020).

727 [25] H. Yuan, P. Dangla, P. Chatellier, T. Chaussadent, Degradation modelling of concrete submitted to  
728 sulfuric acid attack, *Cement and Concrete Research* 53 (2013) 267-277.

729 [26] R.E. Beddoe, H.W. Dorner, Modelling acid attack on concrete: Part I. The essential mechanisms,  
730 *Cement and Concrete Research* 35(12) (2005) 2333-2339.

731 [27] S.A. Bernal, E.D. Rodríguez, R. Mejía de Gutiérrez, J.L. Provis, Performance of alkali-activated slag  
732 mortars exposed to acids, *Journal of Sustainable Cement-Based Materials* 1(3) (2012) 138-151.

733 [28] R.R. Lloyd, J.L. Provis, J.S.J. van Deventer, Acid resistance of inorganic polymer binders. 1.  
734 Corrosion rate, *Materials and Structures* 45(1) (2012) 1-14.

735 [29] S. Zhang, A. Keulen, K. Arbi, G. Ye, Waste glass as partial mineral precursor in alkali-activated  
736 slag/fly ash system, *Cement and Concrete Research* 102 (2017) 29-40.

737 [30] T. Yang, H. Zhu, Z. Zhang, X. Gao, C. Zhang, Q. Wu, Effect of fly ash microsphere on the rheology  
738 and microstructure of alkali-activated fly ash/slag pastes, *Cement and Concrete Research* 109 (2018)  
739 198-207.

740 [31] X. Gao, Q. Yu, H. Brouwers, Reaction kinetics, gel character and strength of ambient temperature  
741 cured alkali activated slag–fly ash blends, *Construction and Building Materials* 80 (2015) 105-115.

742 [32] K. Goretta, N. Chen, F. Gutierrez-Mora, J. Routbort, G. Lukey, J. Van Deventer, Solid-particle  
743 erosion of a geopolymer containing fly ash and blast-furnace slag, *Wear* 256(7-8) (2004) 714-719.

744 [33] A. Wardhono, D.W. Law, A. Strano, The strength of alkali-activated slag/fly ash mortar blends at  
745 ambient temperature, *Procedia Engineering* 125 (2015) 650-656.

746 [34] A.R. Brough, A. Atkinson, Sodium silicate-based, alkali-activated slag mortars: Part I. Strength,  
747 hydration and microstructure, *Cement and Concrete Research* 32(6) (2002) 865-879.

748 [35] T.A. Aiken, J. Kwasny, W. Sha, M.N. Soutsos, Effect of slag content and activator dosage on the  
749 resistance of fly ash geopolymer binders to sulfuric acid attack, *Cement and Concrete Research* 111  
750 (2018) 23-40.

751 [36] A. Bertron, G. Escadeillas, J. Duchesne, Cement pastes alteration by liquid manure organic acids:  
752 chemical and mineralogical characterization, *Cement and Concrete Research* 34(10) (2004) 1823-1835.

753 [37] F. Puertas, S. Martínez-Ramírez, S. Alonso, T. Vazquez, Alkali-activated fly ash/slag cements:  
754 strength behaviour and hydration products, *Cement and concrete research* 30(10) (2000) 1625-1632.

755 [38] F. Puertas, A. Fernández-Jiménez, Mineralogical and microstructural characterisation of alkali-  
756 activated fly ash/slag pastes, *Cement and Concrete composites* 25(3) (2003) 287-292.

757 [39] I. Ismail, S.A. Bernal, J.L. Provis, R. San Nicolas, S. Hamdan, J.S.J. van Deventer, Modification of  
758 phase evolution in alkali-activated blast furnace slag by the incorporation of fly ash, *Cement and*  
759 *Concrete Composites* 45 (2014) 125-135.

760 [40] A. Adam, Strength and durability properties of alkali activated slag and fly ash-based geopolymer  
761 concrete, School of Civil, Environmental and Chemical Engineering, RMIT University, 2009.

762 [41] N. Lee, H. Lee, Influence of the slag content on the chloride and sulfuric acid resistances of alkali-  
763 activated fly ash/slag paste, *Cement and Concrete Composites* 72 (2016) 168-179.

764 [42] W. Zhang, X. Yao, T. Yang, Z. Zhang, The degradation mechanisms of alkali-activated fly ash/slag  
765 blend cements exposed to sulphuric acid, *Construction and Building Materials* 186 (2018) 1177-1187.

766 [43] D.M. Roy, W. Jiang, M.R. Silsbee, Chloride diffusion in ordinary, blended, and alkali-activated  
767 cement pastes and its relation to other properties, *Cement and Concrete Research* 30(12) (2000) 1879-  
768 1884.

769 [44] I. Ismail, S.A. Bernal, J.L. Provis, S. Hamdan, J.S. van Deventer, Drying-induced changes in the  
770 structure of alkali-activated pastes, *Journal of Materials Science* 48(9) (2013) 3566-3577.

771 [45] ASTM C642, Standard test method for density, absorption, and voids in hardened concrete, ASTM  
772 International, 100 Barr Harbor Drive, PO Box C700, West Conshohocken, PA 19428–2959, United  
773 States, 2008.

774 [46] C. ASTM, 1585-04. Standard test method for measurement of rate of absorption of water by  
775 hydraulic-cement concretes, ASTM International (2004).

776 [47] A. ASTM, C109/C109M-Standard Test Method for Compressive Strength of Hydraulic Cement  
777 Mortars (Using 2-in. or (50-mm) Cube Specimens); 2013. 2, Scope of work shall include but not be  
778 limited to the following:-Suspended metal grid for acoustical tile ceiling system (1999).

779 [48] T. Bakharev, Resistance of geopolymer materials to acid attack, *Cement and Concrete Research*  
780 35(4) (2005) 658-670.

781 [49] L.T. Angenent, K. Karim, M.H. Al-Dahhan, B.A. Wrenn, R. Domínguez-Espinosa, Production of  
782 bioenergy and biochemicals from industrial and agricultural wastewater, *TRENDS in Biotechnology*  
783 22(9) (2004) 477-485.

784 [50] S. Wallah, B.V. Rangan, Low-calcium fly ash-based geopolymer concrete: Long-term properties,  
785 Curtin University of Technology, 2006.

786 [51] Y. Zuo, M. Nedeljković, G. Ye, Pore solution composition of alkali-activated slag/fly ash pastes,  
787 *Cement and Concrete Research* 115 (2019) 230-250.

788 [52] B. Huber, H. Hilbig, M.M. Mago, J.E. Drewes, E. Müller, Comparative analysis of biogenic and  
789 chemical sulfuric acid attack on hardened cement paste using laser ablation-ICP-MS, *Cement and*  
790 *Concrete Research* 87 (2016) 14-21.

791 [53] C. Magniont, M. Coutand, A. Bertron, X. Cameleyre, C. Lafforgue, S. Beaufort, G. Escadeillas, A  
792 new test method to assess the bacterial deterioration of cementitious materials, *Cement and Concrete*  
793 *Research* 41(4) (2011) 429-438.

794 [54] A. Bertron, J. Duchesne, G. Escadeillas, Attack of cement pastes exposed to organic acids in  
795 manure, *Cement and Concrete Composites* 27(9-10) (2005) 898-909.

796 [55] M. Hossain, M. Karim, M. Hasan, M. Hossain, M.F.M. Zain, Durability of mortar and concrete made  
797 up of pozzolans as a partial replacement of cement: A review, *Construction and Building Materials* 116  
798 (2016) 128-140.

799 [56] L. Pel, K. Kopinga, E.F. Kaasschieter, Saline absorption in calcium-silicate brick observed by NMR  
800 scanning, *Journal of Physics D: Applied Physics* 33(11) (2000) 1380.

801 [57] M. Fournier, M. Odorico, E. Nicoleau, A. Ull, P. Frugier, S. Gin, Reactive Surface of Glass Particles  
802 Under Aqueous Corrosion, *Procedia Earth and Planetary Science* 17 (2017) 257-260.

803 [58] S.S. International Organization for Standardization. Technical Committee ISO/TC 24. Particle  
804 characterization including sieving, Particle characterization, Determination of the Specific Surface  
805 Area of Solids by Gas Adsorption: BET Method, ISO2010.

806 [59] E.C. Arvaniti, M.C. Juenger, S.A. Bernal, J. Duchesne, L. Courard, S. Leroy, J.L. Provis, A. Klemm, N.  
807 De Belie, Determination of particle size, surface area, and shape of supplementary cementitious  
808 materials by different techniques, *Materials and Structures* 48(11) (2015) 3687-3701.

809 [60] J.L. Bell, P.E. Driemeyer, W.M. Kriven, Formation of ceramics from metakaolin - based  
810 geopolymers. Part II: K - based geopolymer, *Journal of the American Ceramic Society* 92(3) (2009)  
811 607-615.

812 [61] D.K. Panesar, J. Francis, Influence of limestone and slag on the pore structure of cement paste  
813 based on mercury intrusion porosimetry and water vapour sorption measurements, *Construction and*  
814 *Building Materials* 52 (2014) 52-58.

815 [62] A. Koenig, A. Herrmann, S. Overmann, F. Dehn, Resistance of alkali-activated binders to organic  
816 acid attack: Assessment of evaluation criteria and damage mechanisms, *Construction and Building*  
817 *Materials* 151 (2017) 405-413.

818 [63] J.J. Beaudoin, V. Ramachandran, A new perspective on the hydration characteristics of cement  
819 phases, *Cement and Concrete research* 22(4) (1992) 689-694.

820 [64] H.M. Jennings, Refinements to colloid model of CSH in cement: CM-II, *Cement and Concrete*  
821 *Research* 38(3) (2008) 275-289.

822 [65] A.J. Allen, J.J. Thomas, H.M. Jennings, Composition and density of nanoscale calcium-silicate-  
823 hydrate in cement, *Nature materials* 6(4) (2007) 311.

824 [66] C. Varga, M. Alonso, R.M. De Gutierrez, J. Mejía, F. Puertas, Decalcification of alkali-activated slag  
825 pastes. Effect of the chemical composition of the slag, *Materials and Structures* 48(3) (2015) 541-555.

826 [67] N. Ukrainczyk, O. Vogt, E.A. Koenders, Reactive transport numerical model for durability of  
827 geopolymer materials, *Adv. Chem. Eng. Sci.* 6(04) (2016) 355.

828 [68] P. Rajan, S. Rajendran, J. Sathiyabama, J.L. Christy, J. Jeyasundari, P. Prabhakar, Corrosion  
829 inhibitors for concrete corrosion-An Overview, *European Chemical Bulletin* 2(1) (2012) 1-8.

830 [69] R. Vera, M. Villarroel, A. Carvajal, E. Vera, C. Ortiz, Corrosion products of reinforcement in  
831 concrete in marine and industrial environments, *Materials Chemistry and Physics* 114(1) (2009) 467-  
832 474.

833 [70] M. Kouřil, P. Novák, M. Bojko, Threshold chloride concentration for stainless steels activation in  
834 concrete pore solutions, *Cement and Concrete Research* 40(3) (2010) 431-436.

835 [71] P. Feng, C. Miao, J.W. Bullard, A model of phase stability, microstructure and properties during  
836 leaching of portland cement binders, *Cement and Concrete Composites* 49 (2014) 9-19.

837 [72] A. Mehta, R. Siddique, Sulfuric acid resistance of fly ash based geopolymer concrete, *Construction*  
838 *and Building Materials* 146 (2017) 136-143.

839 [73] S. Thokchom, Fly ash geopolymer pastes in sulphuric acid, *Int. J. Eng. Innovation Res* 3(6) (2014)  
840 943-947.

841 [74] O. Oueslati, J. Duchesne, Resistance of blended cement pastes subjected to organic acids:  
842 Quantification of anhydrous and hydrated phases, *Cement and Concrete Composites* 45 (2014) 89-  
843 101.

844 [75] N.M. Ukrainczyk, M.; Vogt, O.; Koenders, E, Geopolymer, Calcium Aluminate, and Portland  
845 Cement-Based Mortars: Comparing Degradation Using Acetic Acid, *materials* 12 (2019) 3115.

846 [76] Li, Zihui, Peethamparan, Sulapha, Leaching resistance of alkali-activated slag and fly ash mortars  
847 exposed to organic acid.

848 [77] A. Fernández - Jiménez, F. Puertas, I. Sobrados, J. Sanz, Structure of calcium silicate hydrates  
849 formed in alkaline - activated slag: influence of the type of alkaline activator, *Journal of the American*  
850 *Ceramic Society* 86(8) (2003) 1389-1394.

851 [78] S.-D. Wang, K.L. Scrivener, Hydration products of alkali activated slag cement, *Cement and*  
852 *Concrete Research* 25(3) (1995) 561-571.

853 [79] M.B. Haha, G. Le Saout, F. Winnefeld, B. Lothenbach, Influence of activator type on hydration  
854 kinetics, hydrate assemblage and microstructural development of alkali activated blast-furnace slags,  
855 *Cement and Concrete Research* 41(3) (2011) 301-310.

856 [80] C.R. Shearer, J.L. Provis, S.A. Bernal, K.E. Kurtis, Alkali-activation potential of biomass-coal co-fired  
857 fly ash, *Cement and Concrete Composites* 73 (2016) 62-74.

858 [81] L. Alarcon-Ruiz, G. Platret, E. Massieu, A. Ehrlicher, The use of thermal analysis in assessing the  
859 effect of temperature on a cement paste, *Cement and Concrete research* 35(3) (2005) 609-613.

860 [82] A. Fernández - Jiménez, A. Palomo, J.Y. Pastor, A. Martin, New cementitious materials based on  
861 alkali - activated fly ash: performance at high temperatures, *Journal of the American Ceramic Society*  
862 91(10) (2008) 3308-3314.

863 [83] H. El Didamony, H.H. Assal, T.M. El Sokkary, H.A. Abdel Gawwad, Kinetics and physico-chemical  
864 properties of alkali activated blast-furnace slag/basalt pastes, *HBRC Journal* 8(3) (2012) 170-176.

865 [84] H.F. Taylor, *Cement chemistry*, Thomas Telford 1997.

866 [85] M.A. Salih, N. Farzadnia, A.A. Abang Ali, R. Demirboga, Development of high strength alkali  
867 activated binder using palm oil fuel ash and GGBS at ambient temperature, *Construction and Building*  
868 *Materials* 93 (2015) 289-300.

869 [86] M. Thiery, G. Villain, P. Dangla, G. Platret, Investigation of the carbonation front shape on  
870 cementitious materials: effects of the chemical kinetics, *Cement and Concrete Research* 37(7) (2007)  
871 1047-1058.

872 [87] N.Y. Mostafa, S.A.S. El-Hemaly, E.I. Al-Wakeel, S.A. El-Korashy, P.W. Brown, Characterization and  
873 evaluation of the hydraulic activity of water-cooled slag and air-cooled slag, *Cement and Concrete*  
874 *Research* 31(6) (2001) 899-904.

875 [88] C. Ruiz-Santaquiteria, J. Skibsted, A. Fernández-Jiménez, A. Palomo, Alkaline solution/binder ratio  
876 as a determining factor in the alkaline activation of aluminosilicates, *Cement and Concrete Research*  
877 42(9) (2012) 1242-1251.

878 [89] F. Puertas, M. Palacios, A. Gil-Maroto, T. Vázquez, Alkali-aggregate behaviour of alkali-activated  
879 slag mortars: Effect of aggregate type, *Cement and Concrete Composites* 31(5) (2009) 277-284.

880 [90] J.A. Gadsden, *Infrared spectra of minerals and related inorganic compounds*, Butterworths 1975.

881 [91] M.B. Haha, B. Lothenbach, G. Le Saout, F. Winnefeld, Influence of slag chemistry on the hydration  
882 of alkali-activated blast-furnace slag—Part II: Effect of Al<sub>2</sub>O<sub>3</sub>, *Cement and Concrete Research* 42(1)  
883 (2012) 74-83.

884 [92] M. Ben Haha, G. Le Saout, F. Winnefeld, B. Lothenbach, Influence of activator type on hydration  
885 kinetics, hydrate assemblage and microstructural development of alkali activated blast-furnace slags,  
886 *Cement and Concrete Research* 41(3) (2011) 301-310.

887 [93] R.L. Frost, S.J. Palmer, Thermal stability of the 'cave' mineral brushite CaHPO<sub>4</sub>· 2H<sub>2</sub>O—Mechanism  
888 of formation and decomposition, *Thermochimica acta* 521(1-2) (2011) 14-17.

889 [94] Q. Zhou, F.P. Glasser, Thermal stability and decomposition mechanisms of ettringite at < 120 C,  
890 *Cement and Concrete Research* 31(9) (2001) 1333-1339.

891 [95] A. Chaipanich, T. Nochaiya, Thermal analysis and microstructure of Portland cement-fly ash-silica  
892 fume pastes, *Journal of Thermal Analysis and Calorimetry* 99(2) (2009) 487-493.

893 [96] A.W. Decho, Overview of biopolymer-induced mineralization: What goes on in biofilms?,  
894 *Ecological Engineering* 36(2) (2010) 137-144.

895 [97] B. Lothenbach, G. Le Saout, E. Gallucci, K. Scrivener, Influence of limestone on the hydration of  
896 Portland cements, *Cement and Concrete Research* 38(6) (2008) 848-860.

897 [98] M. Zajac, A. Rossberg, G. Le Saout, B. Lothenbach, Influence of limestone and anhydrite on the  
898 hydration of Portland cements, *Cement and Concrete Composites* 46 (2014) 99-108.

899 [99] B. Dilnesa, B. Lothenbach, G. Le Saout, G. Renaudin, A. Mesbah, Y. Filinchuk, A. Wichser, E.  
900 Wieland, Iron in carbonate containing AFm phases, *Cement and Concrete Research* 41(3) (2011) 311-  
901 323.

902 [100] T. Nochaiya, W. Wongkeo, K. Pimraksa, A. Chaipanich, Microstructural, physical, and thermal  
903 analyses of Portland cement-fly ash-calcium hydroxide blended pastes, *Journal of thermal analysis*  
904 *and calorimetry* 100(1) (2009) 101-108.

- 905 [101] N. Marjanović, M. Komljenović, Z. Baščarević, V. Nikolić, R. Petrović, Physical–mechanical and  
906 microstructural properties of alkali-activated fly ash–blast furnace slag blends, *Ceramics International*  
907 41(1, Part B) (2015) 1421-1435.
- 908 [102] A. Bertron, J. Duchesne, G. Escadeillas, Accelerated tests of hardened cement pastes alteration  
909 by organic acids: analysis of the pH effect, *Cement and Concrete Research* 35(1) (2005) 155-166.
- 910 [103] J. Temuujin, A. Minjigmaa, M. Lee, N. Chen-Tan, A. van Riessen, Characterisation of class F fly  
911 ash geopolymer pastes immersed in acid and alkaline solutions, *Cement and Concrete Composites*  
912 33(10) (2011) 1086-1091.
- 913 [104] N. Lee, H. Lee, Reactivity and reaction products of alkali-activated, fly ash/slag paste,  
914 *Construction and Building Materials* 81 (2015) 303-312.
- 915 [105] S.M. Park, J.G. Jang, N. Lee, H.-K. Lee, Physicochemical properties of binder gel in alkali-activated  
916 fly ash/slag exposed to high temperatures, *Cement and Concrete Research* 89 (2016) 72-79.
- 917 [106] S.A. Bernal, J.L. Provis, B. Walkley, R. San Nicolas, J.D. Gehman, D.G. Brice, A.R. Kilcullen, P.  
918 Duxson, J.S.J. van Deventer, Gel nanostructure in alkali-activated binders based on slag and fly ash,  
919 and effects of accelerated carbonation, *Cement and Concrete Research* 53 (2013) 127-144.
- 920 [107] M. Königsberger, J. Carette, Validated hydration model for slag-blended cement based on  
921 calorimetry measurements, *Cement and Concrete Research* 128 (2020) 105950.
- 922 [108] B. Johannesson, Nonlinear transient phenomena in porous media with special regard to concrete  
923 and durability, *Advanced Cement Based Materials* 6(3-4) (1997) 71-75.
- 924 [109] J.S. Van Deventer, J.L. Provis, P. Duxson, Technical and commercial progress in the adoption of  
925 geopolymer cement, *Minerals Engineering* 29 (2012) 89-104.
- 926 [110] L. De Windt, P. Devillers, Modeling the degradation of Portland cement pastes by biogenic  
927 organic acids, *Cement and Concrete Research* 40(8) (2010) 1165-1174.

928

929

930

931